Incorporating a prognostic representation of marine nitrogen fixers into the global ocean biogeochemical model HAMOCC

Hanna Paulsen[1,2], Tatiana Ilyina[1], Katharina D. Six[1], Irene Stemmler[1]

A prognostic representation of N2 fixers is incorporated into the global ocean biogeochemical model HAMOCC

The resulting spatial and temporal patterns of N2 fixation compare well with observations

The sensitivity of prognostic N2 fixers to selected model parameters is tested

H.Paulsen, Max Planck Institute for Meteorology, Bundesstr. 53, 20146 Hamburg, Germany (hanna.paulsen@mpimet.mpg.de).

[1]Max Planck Institute for Meteorology,
Bundesstr. 53, 20146 Hamburg, Germany

[2]International Max Planck Research
School on Earth System Modelling,
Hamburg, Germany

This article has been accepted for publication and undergone full peer review but has not been through the copyediting, typesetting, pagination and proofreading process which may lead to differences between this version and the Version of Record. Please cite this article as an 'Accepted Article', doi: 10.1002/2016MS000737

Abstract.

Nitrogen (N_2) fixation is a major source of bioavailable nitrogen to the euphotic zone, thereby exerting an important control on ocean biogeochemical cycling. This paper presents the incorporation of prognostic N_2 fixers into the Hamburg Ocean Carbon Cycle model (HAMOCC), a component of the Max Planck Institute Earth System Model (MPI-ESM). Growth dynamics of N_2 fixers in the model are based on physiological characteristics of the cyanobacterium *Trichodesmium*. The applied temperature dependency confines diazotrophic growth and N_2 fixation to the tropical and subtropical ocean roughly between 40°S and 40°N. Simulated large scale spatial patterns compare well with observations, and the global N_2 fixation rate of 135.6 Tg N yr^{-1} is within the range of current estimates. Also the vertical distribution of N_2 fixation matches well the observations, with a major fraction of about 85% occurring in the upper 20 m. The observed seasonal variability at the stations BATS and ALOHA is reasonably reproduced, with highest fixation rates in northern summer/fall. Iron limitation was found to be an important factor in controlling the simulated distribution of N_2 fixation, especially in the Pacific Ocean.

The new model component considerably improves the representation of present-day N_2 fixation in HAMOCC. It provides the basis for further studies on the role of diazotrophs in global biogeochemical cycles, as well as on the response of N_2 fixation to changing environmental conditions.

1. Introduction

Nitrogen (N_2) fixation is a major source of 'new' nitrogen to the euphotic zone that is thought to mostly compensate the loss through denitrification, therefore playing a key role in controlling the oceanic nitrogen inventory [e.g., *Karl and Letelier*, 2008]. Since nitrogen limits primary production in large parts of the world's ocean [e.g., *Gruber and Sarmiento*, 1997; *Falkowski*, 1997], the input of 'new' nitrogen by means of N_2 fixation affects the efficiency of the biological pump, and hence the carbon cycle. The process of N_2 fixation, however, is often either neglected, or only poorly represented in the ocean biogeochemistry components of state-of-the-art Earth system models used for climate projections. This is also the case for the Hamburg Ocean Carbon Cycle Model (HAMOCC), the ocean biogeochemical component of the Max Planck Institute Earth System Model (MPI-ESM). Here, we present the incorporation of prognostic N_2 fixers into HAMOCC, aiming at improving the representation of present-day N_2 fixation in the model.

Only specific heterotrophic and autotrophic marine organisms, called diazotrophs, have the capacity to utilize N_2 for metabolic processes. In our study, we focus on the autotrophic types since heterotrophic diazotrophs are still poorly understood and their contribution to global N_2 fixation is unclear [*Zehr et al.*, 2001; *Langlois et al.*, 2005]. There are three main groups of autotrophic diazotrophs, (1) the large, non-heterocystous cyanobacterium *Trichodesmium* [*Carpenter and Romans*, 1991; *Capone et al.*, 1997; *Karl et al.*, 2002; *LaRoche and Breitbarth*, 2005], (2) small-sized unicellular cyanobacteria [*Zehr et al.*, 2001], and (3) symbiont heterocystous diazotrophs associated with diatoms (DDA) [*Carpenter et al.*, 1999; *Foster and Zehr*, 2006]. The ability to fix N_2 ensures diazotrophs

their ecological success throughout vast areas of the tropical and subtropical oceans [*Luo et al.*, 2012]. Recent estimates of global N_2 fixation rates span a large range of about 80 to 200 Tg N yr^{-1} [e.g., *Karl et al.*, 2002; *Großkopf et al.*, 2012], assigning diazotrophy a considerable supply of fixed nitrogen to the euphotic zone on the global scale [*Galloway et al.*, 2004; *Gruber*, 2004].

In the future, the ecological niche of N_2 fixers may increase. Model studies project warmer sea surface temperatures, associated with intensified vertical stratification and reduced supply of nutrients from depth [e.g., *Breitbarth et al.*, 2007]. While these conditions are unfavorable for non-diazotrophic phytoplankton [e.g., *Doney*, 2006; *Boyce et al.*, 2010; *Bopp et al.*, 2013], they could favor the growth of N_2 fixers [*Boyd and Doney*, 2002; *Doney*, 2006; *Paerl et al.*, 2008]. In addition, there is evidence that higher oceanic carbon dioxide (CO_2) concentrations will further stimulate the growth of *Trichodesmium* [*Barcelos e Ramos et al.*, 2007; *Hutchins et al.*, 2007; *Levitan et al.*, 2007]. Due to the coupling of the nitrogen to the carbon cycle, these climatic induced changes in N_2 fixation might impact on the ocean's carbon sequestration capacity [e.g., *Capone*, 2001], which, in turn, affects climate.

The majority of the current generation of global climate-biogeochemical models in the 5^{th} phase of the Coupled Model Intercomparison Project (CMIP5, http://cmip-pcmdi.llnl.gov/) do not account for N_2 fixation nor the loss through denitrification at all [e.g., *Palmer and Totterdell*, 2001; *Vichi et al.*, 2007; *Collins et al.*, 2011; *Watanabe et al.*, 2011]. Only a few CMIP5 models include an explicit representation of N_2 fixers [*Moore et al.*, 2004; *Dunne et al.*, 2013]. The respective parameterizations consider the main relevant characteristics of diazotrophs, such as a relatively slow growth rate and no

growth limitation by nitrogen. Still, these models have deficiencies in either reproducing a reasonable global N_2 fixation [*Moore et al.*, 2004], or the spatial distribution of N_2 fixation [*Dunne et al.*, 2013]. Several one-dimensional [e.g., *Hood et al.*, 2001; *Fennel et al.*, 2002], as well as regional and global models [e.g., *Hood et al.*, 2004; *Moore and Doney*, 2007; *Sonntag*, 2013; *Landolfi et al.*, 2015], take into account additional distinct physiological characteristics of N_2 fixers, such as a specific temperature dependence of diazotrophic growth, or buoyancy. These parameterizations are mostly based on the physiology of the best studied, surface bloom forming marine nitrogen fixer *Trichodesmium* [e.g., *Capone et al.*, 1997, 2005]. The models succeed in simulating regional spatial and temporal patterns of N_2 fixation. The studies of *Monteiro et al.* [2010, 2011] include all three main diazotroph types (*Trichodesmium*, unicellular cyanobacteria, and symbiotic diazotrophs) by means of a "self-assembling" phytoplankton community. In their global model, the three diazotroph types largely co-exist. The authors state that N_2 fixation in the ocean can possibly be represented to a great extent by a model based solely on *Trichodesmium*.

In HAMOCC, the global ocean biogeochemistry model of the MPI-ESM, N_2 fixation has hitherto been represented by a diagnostic formulation. Thereby, the nitrate influx into the surface layer is a function of the nitrate deficit relative to phosphate (derived theoretically based on phosphate concentrations and the Redfield ratio), multiplied by a constant fixation rate [*Ilyina et al.*, 2013]. Although this simplified approach yields a reasonable global N_2 fixation, the observed spatial patterns are not captured. The areas of N_2 fixation are rather coupled to the upwelling areas of nitrate-depleted waters, similar to what can be found in the geochemical model approach of *Deutsch et al.* [2007]. Large fixation rates in HAMOCC occur in high latitudes, which is in contradiction with

observations. Furthermore, the whole influx due to N_2 fixation is prescribed to take place in the first model layer (12 m), in contrast to observations which rather indicate considerable fixation rates down to greater depth levels [e.g., *Davis and McGillicuddy*, 2006; *Luo et al.*, 2012]. Besides the deficiencies in simulating the spatial distribution (horizontally and vertically), the temporal variability is also not captured. The diagnostic formulation is not able to simulate a realistic seasonal cycle due to its tight coupling to upwelling and due to the lacking explicit growth dynamics of N_2 fixers.

Here, we replace the diagnostic formulation of N_2 fixation in HAMOCC by including a prognostic representation of diazotrophs. As the ecological niche of diazotrophs is thought to be to a large extent represented by physiological characteristics of *Trichodesmium* [*Monteiro et al.*, 2010, 2011], we base the formulation of growth dynamics on the physiology of this most abundant and widely studied open ocean diazotroph. The aim of this comprehensive approach is to realistically represent the process of N_2 fixation and its effects on biogeochemical cycles in the global biogeochemical model. This paper provides a detailed description of the parameterization of prognostic N_2 fixers, as well as an analysis and evaluation of the model performance on the basis of observations and previous model studies. Successfully reproducing today's state of N_2 fixation is a prerequisite for capturing its response to future climate. Moreover, the new model component in HAMOCC provides the basis for further studies on the role of diazotrophs in ocean biogeochemical cycles, and on the response of N_2 fixation to different environmental factors.

The remaining paper is organized as follows: Section 2 gives a short overview of the main aspects of the global biogeochemical model HAMOCC, followed by a detailed description of the parameterization of the newly implemented N_2 fixers. The section includes

the model setup and experimental design. Section 3 provides an evaluation of modeled N_2 fixers and N_2 fixation against observations and results from biogeochemical models. Differences in biogeochemistry between two model runs, one with and one without prognostic N_2 fixers, are discussed in Section 4. The sensitivity of N_2 fixers to selected model parameters is assessed in additional experiments (Section 5). The paper closes with a summary and conclusions, discussing the strengths and contraints of the new model component (Section 6).

2. Model description

2.1. The ocean biogeochemical model HAMOCC

The global ocean biogeochemistry model HAMOCC, as part of the MPI-ESM, serves to quantify the uptake and storage of CO_2 in the ocean. HAMOCC includes biogeochemical processes in the water column, the sediment, and at the air-sea interface. The present study extends the version HAMOCC 5.2, which was used as part of the MPI-ESM in the CMIP5 experiments [*Ilyina et al.*, 2013].

Biogeochemical tracers in the water column are fully advected, mixed and diffused by the flow field of the physical model. Biogeochemistry dynamics, which are premised on an extended NPZD (nutrients, phytoplankton, zooplankton, detritus) model approach [*Six and Maier-Reimer*, 1996], include the compartments nutrients (phosphate, nitrate, and iron), oxygen, silicate, phytoplankton, zooplankton, dissolved organic matter, and detritus. Organic material is composed following a constant Redfield ratio of carbon ($C:N:P:O_2 = 122:16:1:-172$) based on *Takahashi et al.* [1985] and of the micronutrient iron ($Fe:P = 366E^{-6}:1$) [*Johnson et al.*, 1997]. The sinking speed of organic matter increases linearly with depth after *Martin et al.* [1987].

Atmospheric deposition of iron is accounted for by applying the present-day climatology of monthly atmospheric dust deposition from *Mahowald et al.* [2006]. It is assumed that a fixed fraction of the dust deposition (3.5 %) is iron, of which 1 % is biologically available.

Denitrification, the reduction of nitrate (NO_3) to N_2 which occurs in suboxic zones, is represented by means of a first order approach with a time constant of 0.00125 d^{-1} in the water column, and 0.01 d^{-1} in the sediment, respectively. This process takes place when oxygen falls below a threshold value of $O_{2_{crit}} = 0.5$ μmol L^{-1} in the water column, and $O_{2_{crit}} = 1$ μmol L^{-1} in the sediment. In the previous model version [*Ilyina et al.*, 2013], N_2 fixation, the conversion of N_2 into bioavailable nitrogen, was realized as a direct input of nitrate to the surface layer with a rate of 0.05 d^{-1} in case of a nitrate to phosphate ratio below the Redfield value of 16 N to 1 P. In this study, the implementation of prognostic diazotrophic growth and related N_2 fixation replaces the diagnostic formulation. The applied parameterization is described in detail in the next subsection (Section 2.2).

2.2. Prognostic parameterization of N_2 fixers

The parameterization of bulk diazotrophic growth is based on observed physiological responses of *Trichodesmium* to environmental conditions. Unicellular cyanobacteria have similar characteristics in many aspects, and thus are not explicitely accounted for. The knowlegde about symbiotic diazotrophs is so limited due to the complex relationship with diatoms that we do not consider them in the parameterization.

Analogous to bulk phytoplankton, N_2 fixers are included as a three dimensional prognostic tracer, advected and mixed by the oceanic flow field of the general circulation model. The governing differential equation describing the dynamics of the N_2 fixers concentration (Diaz) is given by

$$\frac{\partial \mathrm{Diaz}}{\partial t} + V\nabla \mathrm{Diaz} - D\mathrm{Diaz} = \sum\nolimits_k \Psi_{BGC}. \quad (1)$$

Hereby, V is the 3D advection vector, D the diffusion operator (both computed in the ocean general circulation model), and Ψ includes the source and sink terms of biogeochemical processes,

$$\Psi_{BGC} = G - M - w_{Diaz}\frac{\partial \mathrm{Diaz}}{\partial z}, \quad (2)$$

where G is growth, and M mortality of N_2 fixers. The last factor in Equation 2 describes changes in the distribution due to vertical movement with the constant buoyancy velocity w_{Diaz}. This natural motility, provided by the presence of gas vesicles [*Walsby*, 1978; *Villareal and Carpenter*, 2003; *Rodier and Le Borgne*, 2008, 2010], gives *Trichodesmium* an advantage compared to bulk phytoplankton in competition for light. Following *Sonntag* [2013], we set the buoyancy velocity to 1 m d^{-1}.

Growth is limited by the physical conditions light (L) [*Karl and Letelier*, 2008; *Luo et al.*, 2014] and temperature (T) [*Breitbarth et al.*, 2007], and by the nutrients iron (Fe) [e.g., *Moore et al.*, 2009] and phosphate (PO_4) [e.g., *Sañudo-Wilhelmy et al.*, 2001]. The resulting growth rate is given by multiplying the maximum growth rate μ_{max} with the respective limiting functions l_L, l_T, l_{Fe}, and l_P:

$$g = \mu_{max} \cdot l_L \cdot l_T \cdot l_{Fe} \cdot l_P. \quad (3)$$

The maximum growth rate of N_2 fixers (both for *Trichodesmium* and unicellular cyanobacteria) is lower compared to bulk phytoplankton due to the energetically costly

process of N_2 fixation. In our model, the maximum growth rate is set to 0.2 d^{-1}, a value in the middle of the observed range for *Trichodesmium* (doubling time 3-5 days, *Capone et al.* [1997]). The actual growth of N_2 fixers biomass per time step is then given by

$$G = g \cdot \text{Diaz.} \tag{4}$$

Light limitation, as for bulk phytoplankton, is calculated following the photosynthetic irradiance curve formulation by *Smith* [1936]:

$$l_L(I_{PAR}) = \frac{\alpha \cdot I_{PAR}(z)}{\sqrt{{\mu_{max}}^2 + \alpha \cdot I_{PAR}(z)^2}}, \tag{5}$$

with α as the initial slope of the photosynthesis versus irradiance curve, and $I_{PAR}(z)$ the vertical field of photosynthetically active radiation (PAR) in the water column. $I_{PAR}(z)$ is parameterized by a bimodal approach based on *Zielinski et al.* [2002]:

$$I_{PAR}(z) = Io_{PAR}\left[\sigma \cdot e^{-z \cdot k_r} + (1-\sigma) \cdot e^{-z \cdot k_w - k_{Chl} \cdot \int_0^z R_{C:Chl} \cdot (Diaz(z') + Phy(z'))dz'}\right]. \tag{6}$$

Here, Io_{PAR} is the incoming photosynthetically active radiation at the sea surface, covering the wavelength range of 400-700 nm. In order to account for the influence of attenuation by clear water as well as the self shading effect of phytoplankton (Phy), the spectrum is divided at 580 nm (prescribed by σ) into two domains: Whereas for longer wavelengths (red domain) attenuation is dominated by sea water with the attenuation coefficient k_r, for shorter wavelengths (blue/green domain) the absorption by chlorophyll (Chl) with the absorption coefficient k_{Chl} is considered in addition to clear water with the absorption coefficient k_w. For simplicity, and because the actual value is not well

constrained by observations, the carbon to chlorophyll ratio ($R_{C:Chl}$) of N_2 fixers in the model is the same as for bulk phytoplankton, namely 60:1 g C (g Chl)$^{-1}$ [*Ilyina et al.*, 2013]. The temperature limitation of growth l_T is described by a modified Gaussian function as used by *Sonntag* [2013], based on observational evidence gained by *Breitbarth et al.* [2007]:

$$l_T(T) = e^{\left[-\frac{(T-T_{opt})^4}{(T_1-T_2\cdot sgn(T-T_{opt}))^4}\right]}. \tag{7}$$

T_{opt} is hereby the optimal temperature for N_2 fixers growth, and T_1 and T_2 describe the distribution around this optimum. The parameter values are chosen as $T_1 = 5.5$ °C and $T_2 = 1$ °C with an optimum temperature $T_{opt} = 27$ °C, reproducing the observed curve for *Trichodesmium* [*Sonntag and Hense*, 2011; *Breitbarth et al.*, 2007]. Not only *Trichodesmium*, but also unicellular cyanobacteria and diazotrophs in general, are thought to favor warm temperatures [e.g., *Falcón et al.*, 2005; *Langlois et al.*, 2005; *Needoba et al.*, 2007].

The growth dependency on the macro nutrient phosphate and micro nutrient iron is formulated explicitly as a multiplicative limiting approach following Michaelis-Menten kinetics:

$$l_{Fe}(\mathrm{Fe}) = \frac{\mathrm{Fe}}{K_{Fe} + \mathrm{Fe}}, \tag{8}$$

$$l_P(\mathrm{PO_4}) = \frac{\mathrm{PO_4}}{K_P + \mathrm{PO_4}}. \tag{9}$$

The iron demand for the process of N_2 fixation is reported to be nearly 10 - 100 times higher than for any other nitrogen assimilation [e.g., *Falkowski et al.*, 1998; *Berman-Frank et al.*, 2001; *Kustka et al.*, 2003]. In the parameterization, we account for this by a high half-saturation constant K_{Fe} of 0.32 nmol Fe m^{-3}. For phosphate a half saturation constant K_P of $1e^{-8}$ kmol P m^{-3} is applied.

The fundamental difference of *our Trichodesmium* based N_2 fixers compared to bulk phytoplankton in the model is, that their growth is not limited by nitrate due to their capability to utilize N_2. However, it is known, that not all of the cells within a colony or along a filament of *Trichodesmium* contain *nifH*, the necessary gene for N_2 fixation [*Lin et al.*, 1998; *Mulholland and Capone*, 2000; *Berman-Frank et al.*, 2001; *Eichner et al.*, 2014]. In preference to the energetic costly process of breaking the N_2 triple bond, *Trichodesmium* rather can obtain significant amounts of nitrogen through uptake of nitrate and ammonium [*Holl and Montoya*, 2005]. In the model, we account for a potential nitrate uptake of diazotrophs by:

$$G_{NO_3}(\mathrm{NO_3}) = min(\mathrm{NO_3} - \mathrm{NO_{3}}_{min}, G \cdot l_{NO_3}) \tag{10}$$

with

$$l_{NO_3}(\mathrm{NO_3}) = \frac{{\mathrm{NO_3}}^2}{{K_N}^2 + {\mathrm{NO_3}}^2}. \tag{11}$$

Nitrate is taken up by the diazotrophs following Michaelis Menten kinetics with quadratic terms. The first term in the minimum expression in Equation 10 prevents nitrate from getting negative ($\mathrm{NO_3}_{min} = 1e^{-11}$ kmol N m^{-3}). For nitrate uptake, a half-

saturation constant of $K_N = 1.6e^{-8}$ kmol N m^{-3} is applied. The residual nitrogen demand required to maintain the prescribed Redfield ratio of 16 N to 1 P is then supplied by N_2, representing the process of N_2 fixation (G_{N_2}):

$$G_{N_2} = G - G_{NO_3} \tag{12}$$

Hence, the ratio of N_2 fixation and nitrate consumption is not prescribed, but evolves dynamically in the model: If no nitrate is available, N_2 fixation is stimulated, whereas it is reduced with increasing nitrate concentration.

As observations indicate that the grazing pressure on *Trichodesmium* is small [*O'Neil and Roman*, 1994; *Hood et al.*, 2001; *Hewson et al.*, 2004], consumption by zooplankton has been omitted. The sink term of N_2 fixers is given by its natural mortality M:

$$M = min(\text{Diaz} - \text{Diaz}_{min}, m_{Diaz} \cdot \text{Diaz}). \tag{13}$$

The dimensional coefficient m_{Diaz} represents the decay rate. The decay rate is not well constrained by observations and is set to a value of 0.1 d^{-1} as a result of the tuning process. This value is within the range of values applied by other model studies (e.g. 0.05 d^{-1}, *Sonntag* [2013]; 0.18 d^{-1}, *Moore et al.* [2004]). In order to guarantee growth at any location, N_2 fixers concentration can not fall below a threshold Diaz_{min} of $1e^{-11}$ kmol P m^{-3}, mimicing spores floating around in the water column.

The resulting linear loss is partitioned between the detritus pool ($f_{DET} = 0.9$), accounting for the sinking part of the organic matter which is reported to be potentially triggered by programmed cell death of *Trichodesmium* blooms [*Bar-Zeev et al.*, 2013], and

the dissolved organic matter (DOM_{Diaz}) pool ($f_{DOM_{Diaz}} = 0.1$). Nitrate is released into the system via remineralization of detritus and DOM. The contribution of N_2 fixers (and phytoplankton in general) to DOM is largely unknown. There is evidence that part of the DOM in the oligotrophic ocean is transformed into recalcitrant DOM [*Jiao et al.*, 2010]. However, the remineralization rate of DOM is in general not well constrained, and we used it as a tuning parameter to achieve a better distribution of surface nitrate in the system. As a result of model tuning, we set the bacterial degradation rate of DOM produced by N_2 fixers ($rem_{DOM\,Diaz}$) to $4e^{-5}$ d^{-1}.

The organic composition of N_2 fixers in the model is analoguos to bulk phytoplankton (C:N:P:O_2 = 122:16:1:-172). With respect to the change of total alkalinity (TA) due to N_2 fixers growth, this means an increase in TA in case of the usage of nitrate, and no change of TA in case of the usage of N_2 [*Wolf-Gladrow et al.*, 2007; *Ilyina et al.*, 2013].

As *Trichodesmium* photosynthetically produces oxygen while fixing N_2 [*Capone et al.*, 1997], oxygen is released during the process of N_2 fixers production in the model. With the assumption of a constant Redfield ratio for all organic material, the amount of released oxygen depends on the source of nitrogen: If N_2 is used for growth the change in oxygen is 148 kmol O_2 per production of 1 kmol P, and for nitrate, it is 172 kmol O_2, respectively.

2.3. Model setup and experimental design

HAMOCC runs as part of the Max Planck Institute Ocean Model (MPIOM), and both are components of the MPI-ESM. MPIOM is a z-coordinate global general circulation model solving the primitive equations under the hydrostatic and Boussinesq approximation on a C-grid with a free surface [*Marsland et al.*, 2003; *Jungclaus et al.*, 2013]. Details on the coupling of HAMOCC and MPIOM are given in *Maier-Reimer et al.* [2005].

The spatial and temporal resolution of HAMOCC is prescribed by MPIOM. In the current study, a configuration referred to as LR (GR15) is applied [*Jungclaus et al.*, 2013]. The bipolar grid, with poles over Antarctica and Greenland, has a horizontal resolution of about 1.5°, gradually varying between 15 km in the Arctic and about 184 km in the tropics. In the vertical, there are 40 unevenly spaced layers with level thicknesses increasing towards the bottom, whereby eight layers are located within the upper 90 m. The time step is 72 minutes.

For our simulations, MPIOM and HAMOCC are forced daily by the surface boundary condition dataset based on the second ECMWF Re-Analysis project (ERA-40, *Simmons and Gibson* [2000], also referred to as OMIP-Forcing [*Röske*, 2005]). In this forcing dataset, the surface conditions are based on bulk formulae, applied on the ERA-40 data covering the time period from 1958-2001. From this data, a mean annual cycle on a daily basis for relevant parameters like windstress, heat- and freshwater fluxes was calculated [*Röske*, 2005]. Continental runoff is determined by means of a runoff model.

Two model simulations were performed, each starting from model state in equilibrium which was achieved in a pre-industrial control simulation performed for CMIP5 [*Ilyina et al.*, 2013]. In the first simulation, we included the prognostic N_2 fixers and run the model to a new quasi-stationary state reached after 2000 years (in the following referenced as PROG). The second simulation serves as control experiment and uses the diagnostic formuation of N_2 fixation (in the following referenced as REF). For all analyses, the mean of the last 100 years is employed.

3. Evaluation of the model results with respect to diazotrophic biomass and N_2 fixation rates

In this section, a description of the mean model state with respect to diazotrophic biomass and N_2 fixation rates is given. After presenting the observational basis for evaluation, the general global patterns are described, followed by a detailed description and evaluation of the individual ocean basins. Furthermore, the vertical distribution, as well as seasonal dynamics of modeled N_2 fixation are discussed in the context of available observations.

3.1. Observational basis

We use the global compilation of observations of cyanobacterial diazotrophic biomass and N_2 fixation rates by *Luo et al.* [2012] (stored in the information system PANGAEA, doi:10.1594/PANGAEA.774851, accessed in May 2016) for model evaluation. The database provides both volumetric, as well as depth-integrated values of biomass and N_2 fixation rates. The biomass data are based on direct measurements of microscopic colony- and trichome-counts of *Trichodesmium*, and cell-counts of heterocystous cyanobacteria. Limited data is also available based on *nifH* gene abundances. However, as the usage of the latter method is accompanied by a high uncertainty [*Luo et al.*, 2012], we focus on the data based on cell-, colony-, and trichome-counts. Most data are based on the dominant cyanobacterium *Trichodesmium*. As the measurements do not cover the full diazotrophic community, the values can be seen as the lower limits of diazotrophic biomass [*Luo et al.*, 2012].

The N_2 fixation rates in the database are mostly corresponding to whole seawater samples. In some cases the rates are measured for specific organisms, i.e. *Trichodesmium*,

unicellular cyanobacteria, or heterocystous cyanobacteria, which are then summed up. Due to a bias in one of the commonly applied measurement methods ($^{15}N_2$ tracer addition), a large number of N_2 fixation rates within the database might be underestimated to a certain degree [*Mohr et al.*, 2010; *Luo et al.*, 2012, 2014]. On the other hand, some individual N_2 fixation rates might be overestimated due to the contamination of some commercial 15-nitrogen (^{15}N) gas stocks used to estimate N_2 fixation rates in the past [*Dabundo et al.*, 2014]. Since our purpose is to evaluate the general patterns of the simulated N_2 fixation, rather than to compare exact numbers with observations, the database can nevertheless be used for our study. However, the methodoligical uncertainty has to be kept in mind. For our model evaluation, we binned the observational data of biomass and N_2 fixation rates onto a 3° x 3° grid and calculated the geometric means of the data in each bin. For surface values, we averaged the available data from the upper 10 m.

Timeseries of monthly values of N_2 fixation rates exist for the monitoring stations ALOHA (A long-Term Oligotrophic Habitat Assessment) in the North Pacific from 2005 to 2010 [*Church et al.*, 2009; *Luo et al.*, 2012], and for BATS (Bermuda Atlantic Time series Study) in the North Atlantic from 1995 to 1997 [*Orcutt et al.*, 2001; *Luo et al.*, 2012]. These timeseries are applied to evaluate the modeled seasonal dynamics of N_2 fixation.

In addition to in situ measurements, geographical information about *Trichodesmium* derived from remote sensing are used in this study for model evaluation [*Gower and Carpenter*, 1992; *Dupouy et al.*, 2000; *Sarangi et al.*, 2005; *Westberry and Siegel*, 2006].

3.2. Mean state of diazotrophic biomass and N_2 fixation rates

3.2.1. Global distribution

Simulated large scale patterns of N_2 fixers biomass (Figures 1a and 1c) and N_2 fixation (Figures 2a and 2c) in PROG are generally consistent with in situ measurements (Figures 1b and 1d, and Figures 2b and 2d, respectively). Surface concentrations reach values of up to $\sim$ 400 mg C m^{-3}, and depth-integrated values up to $\sim$ 7000 mg C m^{-2}. Surface N_2 fixation rates show values up to $\sim$ 300 μmol N m^{-3} d^{-1}, and depth-integrated values up to $\sim$ 5000 μmol N m^{-2} d^{-1}. The modeled habitat of diazotrophs is confined to tropical and subtropical waters approximately between 40°S - 40°N. The meridional extent and gradient is mainly determined by surface temperature (Figure 4c) and solar radiation (not shown), which are the physical factors directly affecting growth of N_2 fixers in the model (Equation 3). In situ [*Luo et al.*, 2012] and remote sensing observations [*Westberry and Siegel*, 2006] support the view that N_2 fixers' main ecological niche is confined to the tropical and subtropical ocean. Also in model studies which include a higher level of diazotrophic diversity [*Monteiro et al.*, 2010, 2011], the diazotroph habitat is restricted to tropical and subtropical waters, whereby not temperature but nutrient availability seems to be the dominant factor here.

The modeled global depth-integrated N_2 fixation rate in the PROG experiment yields 135.6 Tg N yr^{-1} (Table 2). This value falls into the range of reported estimates of $\sim$ 80 - 200 Tg N yr^{-1}. In general, the estimates based on extrapolations of direct measurements are markedly smaller ($<$ 100 Tg N yr^{-1}, e.g., *Capone et al.* [1997]; *Luo et al.* [2012]) than the geochemical estimates derived from stoichiometric ratios ($>$ 100 Tg N yr^{-1}, e.g., *Gruber and Sarmiento* [1997]; *Deutsch et al.* [2007]). Overall, the global N_2 fixation rate in our model is consistent with the value of 140 Tg N yr^{-1} which has become widely accepted based on recent literature [e.g., *Gruber and Galloway*, 2008; *Voss et al.*, 2013].

With regard to the standing stock of diazotrophs, *Luo et al.* [2012] give different estimates ranging from about 2 Tg C (based on cell counts) to 590 Tg C (based on *nifH*-based abundances). However, the assumptions to derive biomass from cell counts and abundances introduce high uncertainties, which can affect the global estimates up to ± 70% [*Luo et al.*, 2012]. In our model, N_2 fixers develop a total biomass of 100 Tg C, which is within the range of the estimates by *Luo et al.* [2012].

Global denitrification (water column and sediment, 141.9 Tg N yr^{-1}) is approximately balanced by global N_2 fixation (135.6 Tg N yr^{-1}). Water column denitrification is restricted to the eastern parts of the Pacific and Atlantic Ocean, and the northern part of the Indian Ocean (Figure 3b). This pattern is in qualitative agreement with in situ studies (Codispoti et al 2001). However, the extents of the denitrification areas are too large due to the overestimated size of the oxygen minimum zones (OMZs), which is a typical issue of global ocean biogeochemistry models [e.g., *Andrews et al.*, 2013; *Cocco et al.*, 2013].

Experiment REF also yields a reasonable global N_2 fixation rate of 132.6 Tg N yr^{-1}. However, the spatial patterns of N_2 fixation are not correct (Figure 3a). N_2 fixation is solely determined by the surface nitrate to phosphate ratio. Thus, highest rates mainly occur in areas of denitrification (which in REF has a similar pattern as in PROG, Figure 3b), as well as in high latitudes, where nitrate-depleted water masses are upwelled to the surface. The major fraction of N_2 fixation is concentrated in the Pacific Ocean, similar to what has been found in the model study of *Deutsch et al.* [2007], in which N_2 fixation is diagnosed by the observed depletion of excess of P relative to the Redfield N quota ($P^* = PO_4 - NO_3/16$). Observations indicate that the upwelling areas are not the major N_2 fixation sites (Figures 2b and 2d). Furthermore, the high fixation rates in high latitudes

in REF (e.g. up to 300 μmol N m^{-2} d^{-1} in the North Pacific), are not supported by observations. It is known that the majority of N_2 fixers rather inhabit warm waters (*Luo et al.* [2012], Figure 2b and 2d). Replacing the diagnostic formulation by the prognostic growth dynamics leads to a decoupling of N_2 fixation from upwelling patterns. Thereby, the high iron limitation plays a crucial role (Figure 4a) since it restricts diazotrophic growth and N_2 fixation to regions of sufficient dust deposition. The impact of iron on modulating the spatial distribution of N_2 fixation is in accordance with previous model studies [*Somes et al.*, 2010; *Weber and Deutsch*, 2014]. Furthermore, physical conditions, such as light and temperature, which were not accounted for in the diagnostic formulation, now influence diazotrophic activity (Figure 4c). The supply of cold, as well as iron depleted water masses to the surface in the eastern upwelling regions of the South Pacific and South Atlantic leads to strong growth limitation and thus to the absence of N_2 fixers in the major denitrification sites.

In the following, the results of PROG for the individual ocean basins are discussed in more detail. Since, due to the temperature limitation, N_2 fixers growth is limited to latitudes between 40°S - 40°N, the descriptions refer to these respective regions in the Atlantic, Pacific and Indian Ocean.

3.2.2. Atlantic Ocean

In the Atlantic Ocean, diazotrophic growth in the model is mainly limited by phosphate (Figure 4b). Iron concentrations are overall high due to the high dust deposition [*Mahowald et al.*, 2006], and hence do not considerably restrict growth of N_2 fixers (Figure 4a). Observational studies support the controlling role of phosphate for N_2 fixers' growth in the Atlantic Ocean [e.g., *Sañudo-Wilhelmy et al.*, 2001; *Ammerman et al.*, 2003].

In the North Atlantic, high modeled values of diazotrophic biomass and N_2 fixation rates are arranged like a band along the northern coast of South America, extending into the Caribbean Sea and the Gulf of Mexico. The North Brazil Current transports phosphate rich surface water from the equatorial upwelling region northward, resulting in low growth limitation along the boundary (Figure 4b). The magnitudes of concentrations and fixation rates here are overall consistent with observations (surface concentrations $\sim$ 10 mg C m^{-3}; depth-integrated concentrations $\sim$ 100 - 1000 mg C m^{-2}, surface fixation rates $\sim$ 10 μmol N m^{-3} d^{-1}, depth-integrated fixation rates $\sim$ 700 μmol N m^{-2} d^{-1}). Also other models are in line with the pattern of high abundances of N_2 fixers along the northern South American coast [*Hood et al.*, 2004; *Moore et al.*, 2004; *Dunne et al.*, 2013].

At the western side of the North Atlantic basin, high modeled surface concentrations and fixation rates reach latitudes of $> 40°$N due to the drift of diazotrophs with the warm water of the Gulf Stream (Figure 4c). This extension to high latitudes along the western boundary agrees with observations (Figures 1b and 2b).

In the downwelling region of the North Atlantic subtropical gyre, modeled values of diazotrophic biomass and fixation rates approach zero due to the strong P-limitation (Figure 4b). Observations, on the contrary, show overall high values of biomass (up to $\sim$ 300 mg C m^{-2}) and fixation rates ($\sim$ 100 μmol N m^{-2} d^{-1}) here. The underestimation of simulated N_2 fixation associated with a too strong P depletion was similarly found in the model study of *Moore et al.* [2004]. It indicates that the parameterizations, which in both models include phosphate limitation, lack a process with respect to the phosphorus source for N_2 fixers growth. There is observational evidence that the utilization of dissolved organic phosphorus (DOP) could provide diazotrophs with sufficient phosphorus

to grow in phosphate depleted regions [*Sohm and Capone*, 2006; *Dyhrman et al.*, 2006]. Model studies support this hypothesis and showed that including the access of diazotrophs to DOP expands their simulated ecological niche into the North Atlantic subtropical gyre [*Somes et al.*, 2010; *Landolfi et al.*, 2015; *Somes and Oschlies*, 2015]. Another proposed mechanism, based on observations, is that N_2 fixers vertically migrate to levels of higher phosphate concentrations in order to meet their phosphorus requirement [*Karl et al.*, 1992]. Furthermore, diazotrophs are known to have a higher N:P ratio than bulk phytoplankton [*Letelier and Karl*, 1998; *Krauk et al.*, 2006; *White et al.*, 2006]. The assumption of a uniform Redfield ratio for all organic material in our model (see Section 2.2) overestimates the phosphorus requirement for diazotrophic growth. This could contribute to the phosphate depletion, and the too strong growth limitation we find in our study.

Among the highest concentrations and fixation rates in the Atlantic basin are found off the westcoast of Africa within the latitudinal range of 20°S to about 20°N. Besides the overall good growth conditions in the equatorial region (high temperatures, high iron and phosphate availability, see Figure 4), the overestimation of the extent of the OMZ and hence denitrification in the eastern equatorial Atlantic leads to upwelling of strongly nitrogen-depleted water masses. This enables diazotrophs to outcompete bulk phytoplankton, which results in high diazotroph concentrations and N_2 fixation rates. North of the equator, the simulated biomass is overestimated compared to observations. Modeled and observed fixation rates accord better. South of the equator, in the Gulf of Guinea, evaluation is restricted due to sparse measurements. The few direct observations give evidence for the abundance of N_2 fixing species in this region (Dandonneau, 1971). Model studies support the picture of the eastern tropical Atlantic being an important

habitat for diazotrophs. In the simulation of *Hood et al.* [2004], the Gulf of Guinea is a hotspot of *Trichodesmium* abundance, mainly controlled by light and MLD. The model of *Moore et al.* [2004], which explicitely accounts for phosphate and iron limitation, also shows high values of N_2 fixation here. In the model study of *Monteiro et al.* [2010], which simulates various diazotrophic groups, all three main types are highly abundant in the equatorial Atlantic, especially in the Gulf of Guinea.

Further to the south, our results show a sharp east-west gradient in concentrations and fixation rates. High abundances in the west are due to the drift of N_2 fixers with the surface current southward along the South American Coast. Whereas the simulated N_2 fixation rates ($\sim$10 μmol N m^{-2} d^{-1}) agree with observations, the biomass concentrations ($\sim$10 mg C m^{-3}) seem to be overestimated by the model. However, since the biomass measurements are mostly restricted to *Trichodesmium*, the actual values for bulk diazotrophs are probably larger. In the east, low temperatures and iron concentrations in the Benguela Upwelling region prevent growth in our model. Measurements of surface concentrations support the absence of diazotrophs in the coastal upwelling area. Data on N_2 fixation, albeit sparse, indicate non-negligible fixation rates in the eastern part of the South Atlantic ($\sim$10 μmol N m^{-2} d^{-1}), about 1000 km away from the coast (Figures 2b and 2d). The simulation of *Monteiro et al.* [2010], which includes various diazotrophic groups, better represents the presence of N_2 fixers in the waters off Southern Africa. However, looking at their pattern of N_2 fixers abundance, this is probably not due to the higher level of diazotrophic diversity in their model, but due to a stronger transport of diazotrophs and warm water from the Indian into the Atlantic Ocean.

3.2.3. Pacific Ocean

Diazotrophic growth in the Pacific Ocean is mainly limited by iron (Figure 4a) and regionally by phosphate (Figure 4b) in our model. An exception with regard to iron limitation is the eastern tropical Pacific north of the equator, where a high atmospheric dust deposition at about 20°N [*Mahowald et al.*, 2006] results in high oceanic surface iron concentrations. The implied low iron limitation (Figure 4a) leads to intense growth (> 100 mg C m^{-2}) and N_2 fixation (> 1000 μmol N m^{-2}) off the coast of North and Central America. In comparison to other dust deposition climatologies [e.g., *Mahowald et al.*, 2003; *Luo et al.*, 2003], the applied climatology of *Mahowald et al.* [2006] shows rather high values in the eastern tropical Pacific, which might cause an overestimation of N_2 fixers' activity in this region. Additionally, the overestimated extent of the OMZ and related denitrification might further support the high diazotroph abundance due to the upwelling of P* enriched water masses. Satellite data support the picture of high concentrations of *Trichodesmium* in the eastern equatorial Pacific [*Westberry and Siegel*, 2006]. Also in situ observations confirm the presence of N_2 fixers, but the observed concentrations and N_2 fixation rates are considerably lower (Figures 1 and 2). However, the only sparse observational data, which in many cases do not represent the full diazotrophic community, can be considered as the lower limit of diazotrophic biomass and N_2 fixation rates [*Luo et al.*, 2012]. Model studies show equivocal results with respect to this region. In the geochemical, diagnostic model of *Deutsch et al.* [2007], the eastern Pacific is a dominant location of N_2 fixation due to the upwelling of nitrogen-deficient waters from the denitrification zone. Also a number of models which include explicit N_2 fixers show a high abundance of diazotrophs in the eastern equatorial Pacific [*Moore and Doney*, 2007; *Dunne et al.*, 2013; *Somes et al.*, 2010; *Landolfi et al.*, 2015]. Other studies rather indicate

low values or even the absence of diazotrophs in this region [*Moore et al.*, 2004; *Monteiro et al.*, 2010]. Discrepancies between the models are probably due to differences in the applied dust deposition climatologies, which vary greatly with respect to the the amount of dust deposition over the eastern Pacific Ocean.

In our model, the N_2 fixers' habitat extends like two zonal bands through the North and South Pacific Ocean at a latitudinal range of about 15 - 25°N and 15 - 25°S. The ability to fix N_2 allows diazotrophs to outcompete bulk phytoplankton within the nitrate-depleted subtropical gyres. Also observations show significant N_2 fixation rates at 20°N - 30°N in the central North Pacific (*Luo et al.* [2012]; Figures 2b and 2d).

In the South Pacific, N_2 fixation in our model is shifted away from the coast. Cold temperatures and low iron concentrations of the water in the upwelling region limit diazotrophic growth, whereby temperature is the dominant factor (Figures 4a and 4c). The fact that considerable N_2 fixation rates were measured here (Figure 2b), might indicate that our parameterization misses diazotrophs which are adapted to colder temperatures. In general, more research is needed on the physiology and the importance of the more uncharacterized N_2 fixing groups (e.g. unicellular cyanobacteria) that grow in cooler water [e.g. *Moisander et al.*, 2010].

In the western Pacific, our model shows a large area of overall high concentrations on an order of 100 - 1000 mg C m^{-2} and fixation rates of 100 - 1000 μmol N m^{-2}. Low nitrate, and sufficient iron and phosphate concentrations promote growth of diazotrophs here. Whereas the high fixation rates fit well to observations, the biomass concentrations, for which only very limited observations are available, seem to be overestimated. However, in the southwestern tropical Pacific off the coast of Australia (at about 20°S), in situ

data based on *nifH*-gene measurements support this high biomass [*Luo et al.*, 2012]. Also satellite measurements have detected *Trichodesmium* blooms in this region [*Dupouy et al.*, 2000]. Moreover, modeling studies agree on the overall high abundance of N_2 fixers in the western part of the Pacific Ocean [e.g., *Moore et al.*, 2004; *Monteiro et al.*, 2010; *Landolfi et al.*, 2015].

The central equatorial Pacific is not inhabited by diazotrophs in our simulation. The upwelling of cold and iron-depleted deep waters limits diazotrophic growth (Figures 4a and 4c) and the concurrent availability of nitrate enables non-fixing phytoplankton to outcompete N_2 fixers. Although the absence of diazotrophs along the equator agrees with measurements of negligible biomass (based on *Trichodesmium* and DDA) (*Luo et al.* [2012], Figure 2b) as well as with the resource-ratio theory of *Ward et al.* [2013], observations of N_2 fixation rather indicate considerable fixation rates of up to a few hundred μmol N m^{-2} at this location (Figure 2d). Again, this discrepancy between the model and observations indicates that the model does not capture the full diazotrophic community. However, also a higher level of diazotrophic diversity as applied in the model study of *Monteiro et al.* [2010] does not reproduce the presence of N_2 fixers in the central equatorial Pacific.

3.2.4. Indian Ocean

In the Indian Ocean, the model produces high surface values of biomass (up to $\sim$ 100 mg C m^{-3}) and N_2 fixation (up to $\sim$ 10 μmol N m^{-3}) throughout the whole ocean basin (Figures 1a and 2a). High dust deposition and hence iron availability (Figure 4a) in combination with upwelling of nitrogen-depleted water from the underlying OMZ result in overall good growth conditions. Phosphate is the main limiting factor

in the Indian Ocean (Figure 4b). In situ observations are only available at a few locations. However, the measurements show globally among the highest values of diazotrophic biomass of > 100 mg C m^{-3} (Figure 1b). It is known that the northeastern monsoon promotes blooms of *Trichodesmium* [*Bergman*, 2001; *Lugomela et al.*, 2002]. Satellite data [*Gower and Carpenter*, 1992; *Sarangi et al.*, 2005; *Westberry and Siegel*, 2006] and other global models [e.g., *Moore et al.*, 2004; *Monteiro et al.*, 2010] further support the potential of the Indian Ocean in playing a significant role in global N_2 fixation.

3.2.5. Vertical distribution

Highest modeled N_2 fixers concentrations and fixation rates are located at the surface, where high light intensities promote diazotrophic growth (Figures 5a and 6). Following the exponential decrease of light, the vertical profiles of modeled concentration and fixation decline rapidly with depth. Biomass declines less rapidly than the fixation rates (Figures 5a), since biomass that is mixed downwards to greater depths is not necessarily able to grow and fix N_2 due to too low light availability. The largest fraction of biomass and fixation is located in the upper 40 m, where 99 % of the total fixation takes place (85 % in the upper 20 m, respectively).

Regionally, the total vertical extent of diazotrophs in the water column varies considerably (Figure 6). Zonally averaged concentrations of > 0.1 mg C m^{-3} reach depths levels between 70 to 110 m in the meridional band of 25°S to 25°N. In general, highest modeled concentrations develop within the mixed layer (Figure 6). Comparing both hemispheres, in the upper 40 m, higher zonally averaged concentrations occur on the northern hemisphere compared to the southern hemisphere (Figure 7). This is probably due to the overall high values present in the eastern tropical North Pacific (Figures 1a and 1c). Ob-

servational evidence regarding the distribution of biomass and fixation rates with depth is equivocal. Several studies, using net tows, found concentrations restricted to the nearest surface [e.g., *Carpenter and Price*, 1977; *McCarthy and Carpenter*, 1979; *Orcutt et al.*, 2001]. However, measurements with a novel optical method revealed a more uniform distribution of *Trichodesmium* colonies over the water column than previously thought [*Davis and McGillicuddy*, 2006], supporting the vertical distribution as simulated by our model. The database of *Luo et al.* [2012] confirms the abundance of diazotrophs and N_2 fixation over greater depths (down to $\sim$ 250 m).

Long-term measurements of the vertical profile of N_2 fixation rates are only available at the ALOHA station, providing values approximately once per month over the period of 2005 - 2010 [*Luo et al.*, 2012]. In general, comparisons between observations at single geographical positions and simulations with a coarse resolution model are difficult. We choose a location in the model with a similar seasonal cycle of sea surface temperature to the one observed at ALOHA, located $\sim 4^\circ$ latitude further south of the actual geographical position. The simulated mean vertical profile of N_2 fixation at this location lies within the range of observed values (Figure 5b). However, the decrease of N_2 fixation with depth is steeper in the model than in observations. The measurements show a quite homogenous profile with considerable fixation rates of about 1 μmol N m^{-3} d^{-1} reaching down to a depth of about 75 m. Whereas the modeled rates in the upper levels (0 - 20 m) fall into the upper range of observations, below a depth of 30 m the model values are rather too small compared to the observed ones. However, it has to be kept in mind, that the ocean model is driven by a climatological forcing, which produces an overall smaller interannual variability in the modeled N_2 fixation rates than present in reality. The high variability of

N_2 fixation existent at this location is indicated by the large standard deviations observed for the single depth levels (Figure 5b). The new parameterization improves the vertical distribution of N_2 fixation rates compared to the diagnostic formulation, in which the total input of 'new' nitrogen was added by definition to the surface layer (for ALOHA: Figure 5b, blue dot).

3.3. Seasonal variability of diazotrophic biomass and N_2 fixation rates

The modeled biomass and fixation rates show a pronounced seasonal cycle, mainly driven by physical conditions like temperature and light. Thereby, the northern and southern boundary of its occurrences move slightly polewards in summer, and equatorwards in winter of the respective hemispheres (by approximately 10° latitude). In the northern hemisphere, highest surface concentrations, as well as shallow reaching biomass occur in August to November (Figure 7a); in the southern hemisphere in December to May (Figure 7b). During winter and spring of the respective hemisphere, enhanced mixing of N_2 fixers downwards, as well as stronger light limitation, lead to lower surface concentrations. The expansions to greater depths due to downward mixing are probably supported by better growth conditions due to a weaker self shading effect (i.e., light absorption by biomass lying above) in the upper layers.

Observed timeseries of biomass and N_2 fixation rates (measured approximately once per month) are available at two locations, the long-term monitoring stations ALOHA [*Church et al.*, 2009; *Luo et al.*, 2012], and BATS [*Orcutt et al.*, 2001; *Luo et al.*, 2012]. Figure 8a shows the observed and modeled N_2 fixation rates at station ALOHA. For the model-observation comparison of the seasonal cycle, we take a model position corresponding to the physical conditions at the location of ALOHA, as already done for the comparison

of the vertical profile (Section 3.2.5). The magnitudes of the modeled prognostic depth-integrated N_2 fixation rates (PROG), and also its seasonal pattern with lowest values at the end/beginning of the year and highest values in the middle of the year, generally agree with the observed ones. However, the peak in the modeled fixation rates occurs too early, in May instead of August. This is caused by a rapid decline of bulk phytoplankton productivity in the model from January onwards, with a minimum in May (not shown). As diazotrophs compete with bulk phytoplankton for phosphate and light, this sharp drop of bulk phytoplankton promotes enhanced growth of diazotrophs too early within the year. Furthermore, the values at the end and beginning of the year (November-March) appear to be underestimated by the model. The N_2 fixation in experiment REF produces higher values during this period which better agree with the observed ones. However, the diagnostic formulation is not able to produce a reasonable seasonal cycle. The monthly mean values do not spread much around the annual mean of 84.7 μmol N m^{-2} d^{-1}, which is generally too low in comparison to the observed annual mean of 126.7 μmol N m^{-2} d^{-1}. The mean fixation rate of PROG with 110.3 μmol N m^{-2} d^{-1} matches the observational record better.

At BATS, long-term measurements of N_2 fixation are only available for the surface seawater. The seasonal cycle of the model results of PROG at the corresponding geographical coordinates are conform with the observed ones, showing highest surface fixation rates from July to October, and lowest, which approach even zero, during the rest of the year (Figure 8b). A discrepancy is seen in September, where observations show a rather low value of 0.02 μmol N m^{-3} d^{-1}, with low standard deviation, whereas the model has its maximum of about 0.1 μmol N m^{-3} d^{-1} in this month. In general, the fixation rates are

rather low at this position, both in observations and in the model. On the contrary, experiment REF strongly overestimates the observed values of surface N_2 fixation at BATS by more than a factor of 20 troughout the whole year (Figure 8b). In the diagnostic formulation, by definition the fixed nitrogen is added to the first model layer. Even if distributing the integrated fixation rate ($\sim$ 21.5 μmol N m^{-2} d^{-1}) over the upper 30 m, the resulting value for the volumetric rate is still too large ($\sim$ 0.72 μmol N m^{-3} d^{-1}). Furthermore, the seasonal cycle is opposite to the observed one. Hence, the diagnostic formulation is neither able to produce fixation rates in the right order of magnitude at this location (see Section 3.2.1), nor a reasonable seasonal cycle.

In the Indian Ocean, PROG shows a pronounced seasonal cycle of N_2 fixers biomass and N_2 fixation rates, with highest values from September to February (not shown). This strong seasonal pattern is also reported from observations, and roughly corresponds to the timing of the monsoon, with highest biomass promoted by the northeast monsoon (November-April) when water conditions are generally calm and warm, and lowest values during the southwest monsoon (June-October) [*Carpenter and Capone*, 1992; *Bergman*, 2001; *Lugomela et al.*, 2002].

The comparison of the results of the two treatments of N_2 fixation (PROG and REF) shows that prognostic growth dynamics are needed to produce reasonable seasonal dynamics of N_2 fixation. In contrast to REF, the variable growth rate in PROG is able to respond to the seasonally changing physical conditions like temperature and light, and acts on the variable standing stock of N_2 fixers instead of prescribing a constant rate.

Besides the pronounced seasonal cycle, variability on shorter timescales is present in the modeled diazotrophic biomass. The temporal evolution of N_2 fixers concentration

shows episodic events of high concentrations which last for a few weeks or even months (not shown). Yet, as the simplification of a linear decay rate in the parameterization neglects mortality of N_2 fixers due to abrupt cell death or viruses which potentially are important [e.g., *Hewson et al.*, 2004], the model does not capture the very short-lived behaviour of blooms reported from observations [e.g., *Bar-Zeev et al.*, 2013]. As a result, the abundances of N_2 fixers in the model may be less patchy and more stable than observed for *Trichodesmium*. Longer durations of blooms up to several months that have been observed [e.g., *Devassy and Goes*, 1988] are better represented in the model.

4. Effects of N_2 fixers on the mean biogeochemical model state

In general, the mean states of both experiments PROG and REF are similar, and comparable to the coupled model run described in detail in *Ilyina et al.* [2013]. However, as the novel prognostic N_2 fixers in PROG affect the other biogeochemical model pools, differences in the fluxes and inventories compared to the simulation with diagnostic N_2 fixation (REF) occur. Concurrently, changes in the biogeochemical state variables between the two model runs emerge. In the following, we discuss differences between the two simulations PROG and REF with regard to fluxes and inventories within the euphotic zone, as well as with regard to state variables. We use observations from the World Ocean Atlas (WOA) 2013 (https://www.nodc.noaa.gov/OC5/woa13/) for evaluation of the state variables. Thereby, we focus on the distribution of nitrate, phosphate, and oxygen, since these are the key variables relevant for biological processes. Iron is not considered, as its spatial pattern is largely determined by the applied dust deposition field. The derived quantity P* ($PO_4 - NO_3/16$), a measure of the excess of P relative to the Redfield N

quota [e.g., *Deutsch et al.*, 2007; *Somes et al.*, 2010], is additionally applied to assess the model skill with respect to phosphate and nitrate.

4.1. Effects on organic matter fluxes and inventories within the euphotic zone

The main fluxes and inventories of the model pools within the euphotic zone of the two experiments are summarized in Table 2. The global annual N_2 fixation rate in the simulation with the prognostic diazotrophs (PROG) of 135.6 Tg N yr^{-1} is similar to the simulation with diagnostic N_2 fixation (REF) with 132.6 Tg N yr^{-1}. In REF, the input of 'new' nitrogen enters by definition directly into the nitrate pool of the surface layer. In PROG N_2 is utilized for the production of diazotrophic biomass, and reaches the nitrate pool indirectly via remineralization. Hence, in contrast to REF, the input of 'new' nitrogen does not exclusively occur in the uppermost model layer. In both simulations global N_2 fixation approximately balances denitrification (141.9 Tg N yr^{-1} in PROG and 135.0 Tg N yr^{-1} in REF).

The bulk phytoplankton standing stock is similar between the two runs (0.62 Gt C in REF and 0.61 Gt C in PROG). Since diazotrophs, unlike bulk phytoplankton, can grow in the nitrate depleted oligotrophic tropical and subtropical oceans, the total standing stock of autotrophs increases to 0.71 Gt C in PROG when adding the diazotrophic biomass of 0.10 Gt C. Globally, N_2 fixers represent about 14 % of the mean phytoplankton biomass. In the tropical regions they often constitute up to 90 %. This large proportion of diazotrophic biomass in distinct regions of the ocean is in accordance with observations [*Capone et al.*, 2005; *Mahaffey et al.*, 2005].

Although the global biomass of bulk phytoplankton is very similar between the two model runs, the global value of net primary production (NPP) by bulk phytoplankton

is considerably lower in PROG (45.53 Gt C yr^{-1}) compared to REF (61.01 Gt C yr^{-1}). This decrease in NPP results from the competition with diazotrophs, which regionally prevail over bulk phytoplankton in the tropics and subtropics. Furthermore, lower nitrate concentrations in high latitudes, as will be discussed in Section 4.1.1, result in stronger growth limitation of bulk phytoplankton and hence additionally reduce NPP. Adding the fraction of NPP produced by N_2 fixers (3.23 Gt C yr^{-1}), yields an overall value of 48.76 Gt C yr^{-1} for the experiment PROG. The global value of NPP is generally not well constrained, and both model states lie within the spread of published estimates ranging from about 40 to 70 Gt C yr^{-1} [e.g., *Carr et al.*, 2006; *Westberry et al.*, 2008].

Along with a smaller NPP in PROG, the fluxes from the phytoplankton pool into the zooplankton pool (grazing) as well as into the DOM pool decrease, together with a decrease in the respective inventories ('DOM': 5.88 Gt C in REF and 4.64 Gt C in PROG; 'ZOO': 0.51 Gt C in REF and 0.39 Gt C in PROG). Accordingly, also the fluxes from bulk phytoplankton and zooplankton into the detritus pool are reduced, whereas the inventory of the detritus pool stays similar (1.62 Gt C in REF and 1.57 Gt C in PROG) due to the contribution from N_2 fixers. Export production in 90 m depth is almost the same in the two experiments (7.24 Gt C yr^{-1} in REF and 7.46 Gt C yr^{-1} in PROG). The difference is negligible against the background of the large range of reported estimates (3-20 Gt C yr, *Najjar et al.* [2007]). The DOC pool fed by diazotrophs (DOM_{Diaz}, 0.82 Gt C) is about 15 % of the total DOC pool (5.44 Gt C). As not much is known about the partitioning of DOM into various refractory pools, it is difficult to evaluate this number.

4.1.1. Effects on the global distribution of nitrate, phosphate, and oxygen

Accounting for diazotroph's dynamics does not fundamentally change the large scale patterns of surface nitrate and phosphate in the model (Figures 9 and 10). But regionally, differences occur. Although the global mean N_2 fixation rate is very similar in the two experiments (Table 2), the spatial distribution of nitrate influx is very different. In REF the nitrate influx takes place almost all over the global ocean (Figure 3) and by definition adds directly nitrate into the surface layer. In PROG, nitrate addition occurs where after N_2 fixation the biomass of diazotrophs is remineralized, thus primarily in the tropical and subtropical ocean (Figures 2a and 2c). As N_2 fixation is absent in high latitudes in PROG, surface nitrate concentrations are lower, regionally up to 2.5 mmol N m^{-3}. In contrast, surface phosphate concentrations are higher here (up to 0.1 mmol P m^{-3}) (Figure 10), since lower nitrate concentrations lead to a decrease of bulk phytoplankton growth in high latitudes. The lower nitrate and higher phosphate concentrations in high latitudes are more realistic, as indicated by comparing simulated spatial patterns of P* to observations (Figure 11). In the process of N_2 fixation, only phosphate and no nitrate is consumed (reducing P*). During growth of non-fixing phytoplankton, in contrast, nitrate and phosphate are consumed proportionally (conserving P*). The absence of N_2 fixation in high latitudes as well as in the central equatorial Pacific in PROG leads to an increase of P* in the respective regions, which is in better agreement with observations than the rather low values present in REF.

In the tropics and subtropics, the upwelling of P* rich water from denitrification sites (Figure 11) promotes N_2 fixation. As discussed above, N_2 fixation then reduces phosphate and P* at the surface. The too strong depletion of surface phosphate and P* in regions of highest N_2 fixation indicates either an overestimation of N_2 fixation in the respective

regions, or a shortcoming in the growth parameterization. An overestimation of N_2 fixation might be caused by too strong denitrification, or, in case of the eastern tropical Pacific, by too high dust deposition. With respect to the model shortcoming, one potential cause for the phosphate and P* depletion could be the low N:P ratio that is prescribed for diazotrophs in the model (see Section 2.2). Furthermore, a missing process in the growth parameterization with respect to the phosphorus source (like dissolved organic phosphorus utilization or the vertical movement to depths of higher phosphate concentrations, as discussed in Section 3.2.2) might be responsible for the strong depletion of phosphate and P* at the surface. Surface nitrate is also more depleted in PROG in the regions of diazotrophic growth compared to REF (regionally up to 0.8 mmol N m^{-3}). This is because the prognostic N_2 fixers first consume the available nitrate before utilizing N_2 for growth. As the physical growth conditions are mostly favorable in the tropical and subtropical regions, diazotrophs grow unhindered until nutrients are exhausted. Thus, although N_2 fixers add 'new' nitrate to the system, the associated production of biomass, and the subsequent sinking of a large fraction of the decaying material (detritus), leads to a depletion of the nitrate in the surface layer, rather than to an accumulation.

Highest differences in nitrate and phosphate between the model runs occur at the surface. Already at a depth of 100 m the concentrations do not differ notably between the two model states (Figures 9 and 10). In case of nitrate, both experiments show generally slightly higher concentrations in the centers of the subtropical gyres compared to observations. In experiment PROG this discrepancy is partly reduced. Below 100 m, in case of phosphate no deviations between the two models are visible (not shown). Differences in oxygen between the two experiments, both at the surface and at 100 m depth, are

marginal and the respective maps are not shown here. Also at greater depth, PROG neither improves the OMZs which are generally too enhanced, nor the nitrate concentrations which are generally too low in HAMOCC [*Ilyina et al.*, 2013].

The overall consistency between the two mean model states is affirmed by a Taylor diagram (Figure 12), which visualizes the model skill compared to observations [*Taylor*, 2001]. In the graphs, the observational dataset (WOA 2013) is represented by a correlation and standard deviation of 1. Deviations from 1 display the discrepancy of the modeled to observed variables. For surface nitrate, the model performance shows a slightly higher mismatch to observations in PROG than in REF. For surface phosphate it is the other way around, PROG slightly reduces the model deficiency. At 100 m, nitrate and phosphate are equally well represented in both experiments. The relation between phosphate and nitrate, measured by P*, is considerably improved in PROG compared to REF. Both at the surface and at a depth of 100 m, the values are closer to 1 in PROG compared to REF. For oxygen, values of standard deviation and correlation are almost identical for both experiments at both depth levels.

5. Sensitivity of prognostic N_2 fixers to selected parameters

A number of biological model parameters, such as the growth and decay rate, as well as the half saturation constants for the uptake of nutrients, have been tuned in order to produce reasonable results with respect to N_2 fixers biomass and fixation rates. As the biological parameters are not well constrained by measurements and can vary between different diazotrophic groups, additional sensitivity experiments have been conducted in order to assess the impact of the uncertainties in these parameters on the model results. The parameters of maximum growth rate and decay rate only modify the magnitudes,

rather than the spatial distribution of N_2 fixers and fixation rates. In contrast, the half saturation constants of iron K_{Fe} and phosphate K_P, which enter the limiting functions of growth (Equation 8 and 9), affect also the spatial patterns. Further, the buoyancy velocity w_{Diaz} affects the vertical distribution of N_2 fixers and fixation rates in the model. The motility is a characteristic feature of *Trichodesmium* and does not apply for the other diazotrophic groups. However, it is of interest to test the sensitivity of the model to the buoyancy velocity since *Trichodesmium* constitutes a considerable portion of the diazotrophic community [e.g., *LaRoche and Breitbarth*, 2005].

Simulations were started from the equilibrium model state described in Section 3.2, and run for another 50 years with the modified parameter values for K_P, K_{Fe}, and w_{Diaz}, respectively. Applied parameter values and the respective model response with regard to N_2 fixation are summarized in Table 3.

5.1. Sensitivity to the half saturation constant of phosphate and iron

For the half saturation constant of phosphate K_P, values of 0.1, 0.5, 2, and 10 times the reference value of K_P=1e^{-8} kmol P m^{-3} were applied (Table 3). They were chosen as to cover a large range of available global estimates of N_2 fixation. An approximate linear relationship between K_P and the resulting global N_2 fixation appears to hold. This can be explained by the hyperbolic form of the applied limiting function following Michaelis Menten kinetics (Equation 9). As the reference value of K_P=1e^{-8} kmol P m^{-3} is in the order of magnitude of the ambient phosphate concentrations, changes around this value result in approximately linear changes in the growth rate. Furthermore, as the horizontal gradients of phosphate are rather small in the area where N_2 fixers occur, this results in an overall linear change of the global N_2 fixation. Decreasing K_P (0.1e^{-8} and

$0.5e^{-8}$ kmol P m^{-3}) leads only to a small increase of overall N_2 fixers concentrations, without a notable change in the inhabited area (Figures 13a and 13b). The global N_2 fixation rate only slightly increases (140.1 and 145.4 Tg N yr^{-1} compared to 135.6 Tg N yr^{-1} in PROG). Increasing K_P ($2e^{-8}$ and $10e^{-8}$ kmol P m^{-3}), on the other hand, shows a more pronounced effect, both on the global N_2 fixation rate (125.6 and 57.1 Tg N yr^{-1} compared to 135.6 Tg N yr^{-1} in PROG), and on the extent of the diazotrophic habitat (Figures 13c and 13d). For a ten times higher K_P, N_2 fixers almost completely vanish in the West Pacific and subtropical South Pacific. Also the North Pacific, the Atlantic, and the Indian Ocean show considerably lower values of depth-integrated biomass.

Analogous to phosphate, values of 0.1, 0.5, 2, and 10 times the reference value of K_{Fe}=0.32 nmol Fe m^{-3} were tested (Table 3). The resulting N_2 fixation rates (except for the highest K_{Fe}) suggest an exponential relationship, indicating the model's sensitivity to this parameter, and to the iron distribution in general. Horizontal gradients are large in the surface iron concentrations, and hence small changes in K_{Fe} lead to large changes in the spatial distribution of N_2 fixers (Figures 13e-h). Largest changes can be seen in the Pacific Ocean, where, except in the east, rather low surface iron concentrations prevail. Decreasing the original K_{Fe} by 0.5 leads to a small increase of the global fixation (145.7 Tg N yr^{-1} compared to 135.6 Tg N yr^{-1}). The increase in global fixation is larger for a tenfold smaller value of K_{Fe} (150.7 Tg N yr^{-1}), mainly visible in the occupation of N_2 fixers of the equatorial Pacific area, where they were not present before (Figures 13e and 13f). With increasing K_{Fe}, the areal extent of N_2 fixers effectively decreases, mainly in the Pacific, where a doubling of K_{Fe} leads to almost vanishing existence of N_2 fixers in the west and south of the basin (Figure 13g). Further increasing K_{Fe} to a 10 times

higher value shrinks the area covered by N_2 fixers to the hotspots of the atmospheric iron input, which are located in the North East Pacific, the Gulf of Guinea, and the Arabian Sea (Figure 13h). The global N_2 fixation in this case yields only 13.7 Tg N yr^{-1}.

The sensitivity experiments indicate that iron limitation is an important controlling factor in the modeled distribution of N_2 fixers, especially in the Pacific Ocean. An increasing iron limitation leads to a decoupling of N_2 fixation from denitrification sites and to a tighter coupling to the atmospheric iron source which is in agreement with the study of *Weber and Deutsch* [2014]. As knowledge about the iron distribution is very limited, especially in the Pacific Ocean, the dependency of the model performance on iron limitation constitutes a source of uncertainty. Furthermore, we include constant half saturation rates for both phosphate and iron in our model. In reality, large (e.g. *Trichodesmium*) and small diazotrophs (e.g. unicellular cyanobacteria) have very different values. Including this diversity could affect the regional spatial patterns of the simulated habitat, as shown in the sensitivity experiments.

5.2. Sensitivity to the buoyancy velocity

The buoyancy velocity of *Trichodesmium* is poorly constrained by observations, and reported values range from even a negative buoyancy velocity (sinking), to a rising rate of about 260 m d^{-1} [*Walsby*, 1978; *Villareal and Carpenter*, 2003; *Guidi et al.*, 2012]. The extreme rising velocities of 200 m d^{-1} and more are probably only rarely reached, and a mean value of 3 m d^{-1} was reported to hold (*Guidi et al.* [2012], and references therein). We tested values between 0 m d^{-1} (no buoyancy), and 50 m d^{-1}, which can be considered as a high value when taken as a global mean. It corresponds to a rising time of only two days to the surface if diazotrophs are mixed down to a depth of 100 m.

Our model results show, that the global N_2 fixation rate is not sensitive to w_{Diaz} (Table 3). First, this is because already for a velocity of 1 m d^{-1} a major fraction of N_2 fixation takes place in the first model layer (12 m). Hence, higher velocities do only slightly modify the global value of N_2 fixation. Second, P-limitation gets stronger with increasing buoyancy velocity, restricting further growth and fixation. Also the global map of depth-integrated biomass shows only minor changes for different applied values of buoyancy velocity (not shown). However, varying w_{Diaz} affects the surface pattern (Figure 14), as well as the vertical profiles of biomass and fixation rates (Figure 15). Global maps of surface N_2 fixers concentrations generally display higher surface concentrations for higher buoyancy velocities. Related to that, the areal extent in the central Pacific with very low concentrations below 0.1 mg C m^{-3} decreases. Maps of zonally averaged biomass for the different applied buoyancy velocities indicate that the surface area covered by concentrations above 10 mg C m^{-3} extends towards higher latitudes with increasing w_{Diaz} (Figure 14). At the same time, the depth range of N_2 fixers abundance gets shallower and more concentrated at the surface. These changes with changing w_c are also reflected by the mean vertical profiles of biomass. Whereas for the case with $w_{Diaz} = 0$ the concentrations in the upper two model layers (22 m) are almost homogenous due to the mixing by the physical model, all experiments with positive w_{Diaz} (already for a velocity of 1 m d^{-1}) start to show a gradient in this depth range, as the buoyancy counteracts the downward mixing. The highest sensitivity of the change of concentration with depth is seen for parameter values between 0 and 1 m d^{-1}, since vertical mixing is in this order of magnitude. Between 1 and 10 m d^{-1} the differences are relatively small, however, the surface concentrations further increase with increasing rising rate.

The current state of knowledge about the vertical distribution of N_2 fixers biomass and fixation rates is limited, however, observations of vertical profiles will probably increase in the future. Our sensitivity experiments indicate that the buoyancy velocity plays a crucial role in influencing the vertical distribution.

6. Summary and Conclusions

N_2 fixation plays a relevant role in ocean biogeochemical cycles and carbon sequestration [e.g., *Capone*, 2001]. Yet, until now N_2 fixation has only been very simplistically represented in HAMOCC, the ocean biogeochemical component of the MPI-ESM. The diagnostic formulation of N_2 fixation used hitherto was solely aimed at compensating the nitrogen loss due to denitrification. The resulting N_2 fixation was closely coupled to the upwelling sites of nitrogen-depleted water masses and neither captured the spatial distribution, nor the seasonal dynamics of observed N_2 fixation. The implementation of prognostic N_2 fixers, as presented in this paper, leads to a considerable improvement of the model's representation of present-day N_2 fixation. The new model component is included in the standard model MPI-ESM1.2, which will be used inter alia in the upcoming CMIP6 experiments.

Our growth paramterization of bulk N_2 fixers is based on physiological characteristics of the cyanobacterium *Trichodesmium*, which are thought to largely represent the ecological niche of N_2 fixers in general [*Monteiro et al.*, 2010, 2011]. N_2 fixers in our model differ from bulk phytoplankton by their ability to use both NO_3 and N_2, a slower maximum growth rate, stronger iron limitation, buoyancy, and a specific optimum temperature range.

The prognostic parameterization reproduces the large scale distribution of autotrophic N_2 fixers biomass and fixation rates, confined to the tropical and subtropical oceans

between 40°S and 40°N. In addition to fixed N deficits, the spatial patterns of N_2 fixation are controlled by temperature, phosphate, and iron limitation, and thus are partially decoupled from the upwelling areas of nitrogen-depleted water masses. The global N_2 fixation rate yields 135.6 Tg N yr^{-1}, which lies within the range of recently reported estimates (80-200 Tg N yr^{-1}, e.g., *Gruber and Galloway* [2008]; *Voss et al.* [2013]).

N_2 fixing diazotrophs are found in the upper 100 m with a major fraction of biomass confined to the upper 40 m, where about 99 % of the total N_2 fixation occurs (85 % in the upper 20 m, respectively). The diazotrophic activity concentrated in the upper tens of meters is in agreement with observations [*Davis and McGillicuddy*, 2006; *Luo et al.*, 2012], and the simulated vertical profile of N_2 fixation at the location of ALOHA matches well the long-term measurements.

The prognostic growth dynamics, responding to seasonal changes in physical conditions and acting on a variable standing stock of N_2 fixers, are capable of producing a reasonable seasonal variability of N_2 fixation. The observed seasonal cycles at the long-term monitoring station BATS and ALOHA with highest fixation rates in northern summer/fall are adequately simulated, though the timing of the peak at ALOHA occurs a few months too early in the model.

The inclusion of N_2 fixers has marginal effects on the surface distribution of nitrate and phosphate. This is due to the changes in the spatial distribution of nitrate influx by N_2 fixation into the upper ocean, and due to the intensified nutrient turnover by the diazotrophic phytoplankton dynamics. However, the large scale patterns of nutrients resemble the observations as in the previous model version without prognostic diazotrophs. The spatial patterns of P* are improved, indicating that the changes in the spatial distribution of

fixed nitrogen input improve the relative abundance of nitrate to phosphate. However, the prescribed low N:P ratio of 16:1 for diazotrophs causes a depletion of P* in areas of high N_2 fixation. The simulated annual net primary production of 48.76 Gt C yr^{-1} and the export production of 7.46 Gt C yr^{-1} are within the reported ranges of 40–70 Gt C yr^{-1} [e.g., *Carr et al.*, 2006; *Westberry et al.*, 2008] and 3–20 Gt C yr^{-1} [*Najjar et al.*, 2007], respectively.

The fact that the essential characteristics of bulk N_2 fixation are captured by the model gives confidence that the main controlling factors are included in the parameterization based on *Trichodesmium*. However, the absence of N_2 fixers at some locations in our simulation where N_2 fixation has actually been measured (e.g. in the central equatorial Pacific and in Peruvian upwelling region in the South Pacific) indicates that the ecological niche of diazotrophs is not completely covered by our growth parameterization. Sensitivity experiments show that different half saturation constants for nutrient uptake of various diazotroph types might be relevant for regional spatial patterns of the total diazotroph habitat. In general, future research on the physiology of more uncharacterized N_2 fixing groups, e.g. symbiotic diazotrophs, and unicellular cyanobacteria that grow in cooler water [e.g. *Needoba et al.*, 2007; *Moisander et al.*, 2010], will potentially give more insights into if and how other diazotrophic groups should be accounted for in the model. Especially for representing the response of N_2 fixers to variability and climate change it might be important to include a higher level of diazotrophic diversity.

The underestimation of simulated N_2 fixers biomass and fixation rates within the North Atlantic subtropical gyre indicates a lacking mechanism that supplies N_2 fixers with sufficient phosphorus to grow in this region. Proposed mechanisms are the ability of *Tri-*

chodesmium to utilize dissolved organic phosphorus [e.g., *Landolfi et al.*, 2015], and a potential vertical migration of *Trichodesmium* from the phosphate depleted surface layer to the phosphate rich thermocline [*Karl et al.*, 1992].

Sensitivity experiments show that iron limitation is an important factor controlling the distribution of diazotrophs and N_2 fixation in our model, especially in the Pacific Ocean. Our model assigns the Eastern Pacific Ocean a large potential for N_2 fixation, mainly driven by a pattern of high dust deposition. As knowledge of dust deposition and the iron cycle is limited, more direct measurements of N_2 fixation are needed to sufficiently evaluate the model results in this part of the ocean.

The high sensitivity of N_2 fixers to iron as found in our study supports the idea that prospective changes in the atmospheric dust deposition might affect the future evolution of global N_2 fixation [e.g., *Krishnamurthy et al.*, 2007, 2009]. Observations indicate that additional physiological sensitivities of N_2 fixers (which are not accounted for in the current model), like pH-dependent growth [e.g., *Barcelos e Ramos et al.*, 2007], and temperature adaptation [*Thomas et al.*, 2012], could also play a role. The parameterization of prognostic N_2 fixers presented in this paper provides the basis for further studies on the influence of different environmental factors on N_2 fixation, which could give indications for the response of N_2fixation to potential conditions in a future climate.

Acknowledgments.

All simulations were performed at the German Climate Computing Center (DKRZ). The authors thank Mathias Heinze for internal review of the original manuscript. We acknowledge the constructive comments and suggestions of Christopher Somes and one anonymous reviewer that helped to improve the manuscript. Primary data and scripts needed to re-

produce the analyses presented in this study are archived by the Max Planck Institute for Meteorology, and will be available by contacting publications@mpimet.mpg.de

References

Ammerman, J. W., R. R. Hood, D. A. Case, and J. B. Cotner (2003), Phosphorus deficiency in the Atlantic: An emerging paradigm in oceanography, *Eos, Transactions American Geophysical Union*, *84*(18), 165–170.

Andrews, O., N. Bindoff, P. Halloran, T. Ilyina, and C. Le Quéré (2013), Detecting an external influence on recent changes in oceanic oxygen using an optimal fingerprinting method, *Biogeosciences*, *10*(3), 1799–1813.

Bar-Zeev, E., I. Avishay, K. D. Bidle, and I. Berman-Frank (2013), Programmed cell death in the marine cyanobacterium *Trichodesmium* mediates carbon and nitrogen export, *The ISME journal*, *7*(12), 2340–2348.

Barcelos e Ramos, J., H. Biswas, K. G. Schulz, J. LaRoche, and U. Riebesell (2007), Effect of rising atmospheric carbon dioxide on the marine nitrogen fixer *Trichodesmium*, *Global biogeochemical cycles*, *21*(2).

Bergman, B. (2001), Nitrogen-fixing cyanobacteria in tropical oceans, with emphasis on the Western Indian Ocean, *South African journal of botany*, *67*(3), 426–432.

Berman-Frank, I., J. T. Cullen, Y. Shaked, R. M. Sherrell, and P. G. Falkowski (2001), Iron availability, cellular iron quotas, and nitrogen fixation in *Trichodesmium*, *Limnology and Oceanography*, *46*(6), 1249–1260.

Bopp, L., L. Resplandy, J. C. Orr, S. C. Doney, J. P. Dunne, M. Gehlen, P. Halloran, C. Heinze, T. Ilyina, R. Séférian, et al. (2013), Multiple stressors of ocean ecosystems

in the 21st century: projections with CMIP5 models, *Biogeosciences*, *10*, 6225–6245.

Boyce, D. G., M. R. Lewis, and B. Worm (2010), Global phytoplankton decline over the past century, *Nature*, *466*(7306), 591–596.

Boyd, P. W., and S. C. Doney (2002), Modelling regional responses by marine pelagic ecosystems to global climate change, *Geophysical Research Letters*, *29*(16).

Breitbarth, E., A. Oschlies, and J. LaRoche (2007), Physiological constraints on the global distribution of *Trichodesmium* - effect of temperature on diazotrophy, *Biogeosciences (BG)*, *4*(1), 53–61.

Capone, D. G. (2001), Marine nitrogen fixation: what's the fuss?, *Current opinion in microbiology*, *4*(3), 341–348.

Capone, D. G., J. P. Zehr, H. W. Paerl, B. Bergman, and E. J. Carpenter (1997), *Trichodesmium*, a globally significant marine cyanobacterium, *Science*, *276*(5316), 1221–1229.

Capone, D. G., J. A. Burns, J. P. Montoya, A. Subramaniam, C. Mahaffey, T. Gunderson, A. F. Michaels, and E. J. Carpenter (2005), Nitrogen fixation by *Trichodesmium* spp.: An important source of new nitrogen to the tropical and subtropical North Atlantic Ocean, *Global Biogeochemical Cycles*, *19*(2).

Carpenter, E. J., and D. G. Capone (1992), Nitrogen fixation in *Trichodesmium* blooms, in *Marine pelagic cyanobacteria: Trichodesmium and other diazotrophs*, pp. 211–217, Springer.

Carpenter, E. J., and C. C. Price (1977), Nitrogen fixation, distribution, and production of *Oscillatoria (Trichodesmium)* spp. in the western Sargasso and Caribbean Seas, *Limnology and Oceanography*, *22*(1), 60–72.

Carpenter, E. J., and K. Romans (1991), Major role of the cyanobacterium Trichodesmium in nutrient cycling in the North Atlantic Ocean., *Science(Washington)*, *254*(5036), 1356–1358.

Carpenter, E. J., J. P. Montoya, J. Burns, M. R. Mulholland, A. Subramaniam, and D. G. Capone (1999), Extensive bloom of a N_2-fixing diatom/cyanobacterial association in the tropical Atlantic Ocean.

Carr, M.-E., M. A. Friedrichs, M. Schmeltz, M. N. Aita, D. Antoine, K. R. Arrigo, I. Asanuma, O. Aumont, R. Barber, M. Behrenfeld, et al. (2006), A comparison of global estimates of marine primary production from ocean color, *Deep Sea Research Part II: Topical Studies in Oceanography*, *53*(5), 741–770.

Church, M. J., C. Mahaffey, R. M. Letelier, R. Lukas, J. P. Zehr, and D. M. Karl (2009), Physical forcing of nitrogen fixation and diazotroph community structure in the North Pacific subtropical gyre, *Global Biogeochemical Cycles*, *23*(2).

Cocco, V., F. Joos, M. Steinacker, T. Frölicher, L. Bopp, J. Dunne, M. Gehlen, C. Heinze, J. Orr, A. Oeschlies, et al. (2013), Oxygen and indicators of stress for marine life in multi-model global warming projections, *Biogeosciences*, *10*, 1849–1868.

Collins, W., N. Bellouin, M. Doutriaux-Boucher, N. Gedney, P. Halloran, T. Hinton, J. Hughes, C. Jones, M. Joshi, S. Liddicoat, et al. (2011), Development and evaluation of an Earth-system model–HadGEM2, *Geoscientific Model Development*, *4*(4), 1051–1075.

Dabundo, R., M. F. Lehmann, L. Treibergs, C. R. Tobias, M. A. Altabet, P. H. Moisander, and J. Granger (2014), The contamination of commercial $^{15}N_2$ gas stocks with ^{15}N–labeled nitrate and ammonium and consequences for nitrogen fixation measurements,

PloS one, *9*(10), e110,335.

Davis, C. S., and D. J. McGillicuddy (2006), Transatlantic abundance of the N_2-fixing colonial cyanobacterium *Trichodesmium*, *Science*, *312*(5779), 1517–1520.

Deutsch, C., J. L. Sarmiento, D. M. Sigman, N. Gruber, and J. P. Dunne (2007), Spatial coupling of nitrogen inputs and losses in the ocean, *Nature*, *445*(7124), 163–167.

Devassy, V., and J. Goes (1988), Phytoplankton community structure and succession in a tropical estuarine complex (central west coast of India), *Estuarine, Coastal and Shelf Science*, *27*(6), 671–685.

Doney, S. C. (2006), Oceanography: Plankton in a warmer world, *Nature*, *444*(7120), 695–696.

Dunne, J. P., J. G. John, E. Shevliakova, R. J. Stouffer, J. P. Krasting, S. L. Malyshev, P. Milly, L. T. Sentman, A. J. Adcroft, W. Cooke, et al. (2013), GFDLs ESM2 Global Coupled Climate–Carbon Earth System Models. Part II: Carbon System Formulation and Baseline Simulation Characteristics*, *Journal of Climate*, *26*(7), 2247–2267.

Dupouy, C., J. Neveux, A. Subramaniam, M. R. Mulholland, J. P. Montoya, L. Campbell, E. J. Carpenter, and D. G. Capone (2000), Satellite captures *Trichodesmium* blooms in the southwestern tropical Pacific, *Eos, Transactions American Geophysical Union*, *81*(2), 13–16.

Dyhrman, S., P. Chappell, S. Haley, J. Moffett, E. Orchard, J. Waterbury, and E. Webb (2006), Phosphonate utilization by the globally important marine diazotroph *Trichodesmium*, *Nature*, *439*(7072), 68–71.

Eichner, M., S. A. Kranz, and B. Rost (2014), Combined effects of different CO_2 levels and N sources on the diazotrophic cyanobacterium *Trichodesmium*, *Physiologia plantarum*,

152(2), 316–330.

Falcón, L. I., S. Pluvinage, and E. J. Carpenter (2005), Growth kinetics of marine unicellular N_2-fixing cyanobacterial isolates in continuous culture in relation to phosphorus and temperature, *Marine Ecology Progress Series*, *285*, 3–9.

Falkowski, P. G. (1997), Evolution of the nitrogen cycle and its influence on the biological sequestration of CO_2 in the ocean, *Nature*, *387*(6630), 272–275.

Falkowski, P. G., R. T. Barber, and V. Smetacek (1998), Biogeochemical controls and feedbacks on ocean primary production, *Science*, *281*(5374), 200–206.

Fennel, K., Y. H. Spitz, R. M. Letelier, M. R. Abbott, and D. M. Karl (2002), A deterministic model for N_2 fixation at stn. ALOHA in the subtropical North Pacific Ocean, *Deep Sea Research Part II: Topical Studies in Oceanography*, *49*(1), 149–174.

Foster, R. A., and J. P. Zehr (2006), Characterization of diatom–cyanobacteria symbioses on the basis of *nifH*, *hetR* and 16S rRNA sequences, *Environmental Microbiology*, *8*(11), 1913–1925.

Galloway, J. N., F. J. Dentener, D. G. Capone, E. W. Boyer, R. W. Howarth, S. P. Seitzinger, G. P. Asner, C. Cleveland, P. Green, E. Holland, et al. (2004), Nitrogen cycles: past, present, and future, *Biogeochemistry*, *70*(2), 153–226.

Gower, G. A. B. J. F., and E. J. Carpenter (1992), Development of algortithms for remote sensing of *Trichodesmium* blooms, *Marine pelagic cyanobacteria: Trichodesmium and other diazotrophs*, *362*, 193.

Großkopf, T., W. Mohr, T. Baustian, H. Schunck, D. Gill, M. M. Kuypers, G. Lavik, R. A. Schmitz, D. W. Wallace, and J. LaRoche (2012), Doubling of marine dinitrogen-fixation rates based on direct measurements, *Nature*, *488*(7411), 361–364.

Gruber, N. (2004), The dynamics of the marine nitrogen cycle and its influence on atmospheric CO_2 variations, in *The ocean carbon cycle and climate*, pp. 97–148, Springer.

Gruber, N., and J. N. Galloway (2008), An Earth-system perspective of the global nitrogen cycle, *Nature*, *451*(7176), 293–296.

Gruber, N., and J. L. Sarmiento (1997), Global patterns of marine nitrogen fixation and denitrification, *Global Biogeochemical Cycles*, *11*(2), 235–266.

Guidi, L., P. H. Calil, S. Duhamel, K. M. Björkman, S. C. Doney, G. A. Jackson, B. Li, M. J. Church, S. Tozzi, Z. S. Kolber, et al. (2012), Does eddy-eddy interaction control surface phytoplankton distribution and carbon export in the North Pacific Subtropical Gyre?, *Journal of Geophysical Research: Biogeosciences*, *117*(G2).

Hewson, I., S. R. Govil, D. G. Capone, E. J. Carpenter, and J. A. Fuhrman (2004), Evidence of *Trichodesmium* viral lysis and potential significance for biogeochemical cycling in the oligotrophic ocean, *Aquatic Microbial Ecology*, *36*(1), 1–8.

Holl, C. M., and J. P. Montoya (2005), Interactions between nitrate uptake and nitrogen fixation in continuous cultures of the marine diazotroph *Trichodesmium* (Cyanobacteria), *Journal of Phycology*, *41*(6), 1178–1183.

Hood, R. R., N. R. Bates, D. G. Capone, and D. B. Olson (2001), Modeling the effect of nitrogen fixation on carbon and nitrogen fluxes at BATS, *Deep Sea Research Part II: Topical Studies in Oceanography*, *48*(8), 1609–1648.

Hood, R. R., V. J. Coles, and D. G. Capone (2004), Modeling the distribution of *Trichodesmium* and nitrogen fixation in the Atlantic Ocean, *Journal of Geophysical Research: Oceans*, *109*(C6).

Hutchins, D., F.-X. Fu, Y. Zhang, M. Warner, Y. Feng, K. Portune, P. Bernhardt, and M. Mulholland (2007), CO_2 control of *Trichodesmium* N_2 fixation, photosynthesis, growth rates, and elemental ratios: Implications for past, present, and future ocean biogeochemistry, *Limnology and Oceanography*, *52*(4), 1293.

Ilyina, T., K. D. Six, J. Segschneider, E. Maier-Reimer, H. Li, and I. Núñez-Riboni (2013), Global ocean biogeochemistry model HAMOCC: Model architecture and performance as component of the MPI-Earth system model in different CMIP5 experimental realizations, *Journal of Advances in Modeling Earth Systems*, *5*(2), 287–315.

Jiao, N., G. J. Herndl, D. A. Hansell, R. Benner, G. Kattner, S. W. Wilhelm, D. L. Kirchman, M. G. Weinbauer, T. Luo, F. Chen, et al. (2010), Microbial production of recalcitrant dissolved organic matter: long-term carbon storage in the global ocean, *Nature Reviews Microbiology*, *8*(8), 593–599.

Johnson, K. S., R. M. Gordon, and K. H. Coale (1997), What controls dissolved iron concentrations in the world ocean?, *Marine Chemistry*, *57*(3), 137–161.

Jungclaus, J., N. Fischer, H. Haak, K. Lohmann, J. Marotzke, D. Matei, U. Mikolajewicz, D. Notz, and J. Storch (2013), Characteristics of the ocean simulations in the Max Planck Institute Ocean Model (MPIOM) the ocean component of the MPI-Earth system model, *Journal of Advances in Modeling Earth Systems*, *5*(2), 422–446.

Karl, D., A. Michaels, B. Bergman, D. Capone, E. Carpenter, R. Letelier, F. Lipschultz, H. Paerl, D. Sigman, and L. Stal (2002), *Dinitrogen fixation in the worlds oceans*, Springer.

Karl, D. M., and R. M. Letelier (2008), Nitrogen fixation-enhanced carbon sequestration in low nitrate, low chlorophyll seascapes, *Marine Ecology Progress Series*, *364*, 257–268.

Karl, D. M., R. Letelier, D. V. Hebel, D. F. Bird, and C. D. Winn (1992), *Trichodesmium* blooms and new nitrogen in the North Pacific gyre, in *Marine pelagic cyanobacteria: Trichodesmium and other diazotrophs*, pp. 219–237, Springer.

Krauk, J. M., T. A. Villareal, J. A. Sohm, J. P. Montoya, and D. G. Capone (2006), Plasticity of N:P ratios in laboratory and field populations of *Trichodesmium* spp., *Aquat. Microb. Ecol.*, *42*, 243–253.

Krishnamurthy, A., J. K. Moore, C. S. Zender, and C. Luo (2007), Effects of atmospheric inorganic nitrogen deposition on ocean biogeochemistry, *Journal of Geophysical Research: Biogeosciences*, *112*(G2).

Krishnamurthy, A., J. K. Moore, N. Mahowald, C. Luo, S. C. Doney, K. Lindsay, and C. S. Zender (2009), Impacts of increasing anthropogenic soluble iron and nitrogen deposition on ocean biogeochemistry, *Global Biogeochemical Cycles*, *23*(3).

Kustka, A. B., S. A. Sañudo-Wilhelmy, E. J. Carpenter, D. Capone, J. Burns, and W. G. Sunda (2003), Iron requirements for dinitrogen- and ammonium-supported growth in cultures of *Trichodesmium* (IMS 101): Comparison with nitrogen fixation rates and iron: carbon ratios of field populations, *Limnology and Oceanography*, *48*(5), 1869–1884.

Landolfi, A., W. Koeve, H. Dietze, P. Kähler, and A. Oschlies (2015), A new perspective on environmental controls of marine nitrogen fixation, *Geophysical Research Letters*, *42*(11), 4482–4489.

Langlois, R. J., J. LaRoche, and P. A. Raab (2005), Diazotrophic diversity and distribution in the tropical and subtropical Atlantic Ocean, *Applied and Environmental Microbiology*, *71*(12), 7910–7919.

LaRoche, J., and E. Breitbarth (2005), Importance of the diazotrophs as a source of new nitrogen in the ocean, *Journal of Sea Research*, *53*(1), 67–91.

Letelier, R. M., and D. M. Karl (1998), *Trichodesmium* spp. physiology and nutrient fluxes in the North Pacific subtropical gyre.

Levitan, O., G. Rosenberg, I. Setlik, E. Setlikova, J. Grigel, J. Klepetar, O. Prasil, and I. Berman-Frank (2007), Elevated CO_2 enhances nitrogen fixation and growth in the marine cyanobacterium *Trichodesmium*, *Global Change Biology*, *13*(2), 531–538.

Lin, S., S. Henze, P. Lundgren, B. Bergman, and E. J. Carpenter (1998), Whole-Cell Immunolocalization of Nitrogenase in Marine Diazotrophic Cyanobacteria, *Trichodesmium* spp., *Applied and Environmental Microbiology*, *64*(8), 3052–3058.

Lugomela, C., T. J. Lyimo, I. Bryceson, A. K. Semesi, and B. Bergman (2002), *Trichodesmium* in coastal waters of Tanzania: diversity, seasonality, nitrogen and carbon fixation, *Hydrobiologia*, *477*(1-3), 1–13.

Luo, C., N. M. Mahowald, and J. Del Corral (2003), Sensitivity study of meteorological parameters on mineral aerosol mobilization, transport, and distribution, *Journal of Geophysical Research: Atmospheres (1984–2012)*, *108*(D15).

Luo, Y.-W., S. Doney, L. Anderson, M. Benavides, I. Berman-Frank, A. Bode, S. Bonnet, K. Boström, D. Böttjer, D. Capone, et al. (2012), Database of diazotrophs in global ocean: abundance, biomass and nitrogen fixation rates, *Earth System Science Data*, *4*(1), 47–73.

Luo, Y.-W., I. D. Lima, D. M. Karl, C. A. Deutsch, and S. C. Doney (2014), Data-based assessment of environmental controls on global marine nitrogen fixation, *Biogeosciences*, *11*, 691–708.

Mahaffey, C., A. F. Michaels, and D. G. Capone (2005), The conundrum of marine N_2 fixation, *American Journal of Science*, *305*(6-8), 546–595.

Mahowald, N., C. Luo, J. Del Corral, and C. S. Zender (2003), Interannual variability in atmospheric mineral aerosols from a 22-year model simulation and observational data, *Journal of Geophysical Research: Atmospheres (1984–2012)*, *108*(D12).

Mahowald, N. M., D. R. Muhs, S. Levis, P. J. Rasch, M. Yoshioka, C. S. Zender, and C. Luo (2006), Change in atmospheric mineral aerosols in response to climate: Last glacial period, preindustrial, modern, and doubled carbon dioxide climates, *Journal of Geophysical Research: Atmospheres (1984–2012)*, *111*(D10).

Maier-Reimer, E., I. Kriest, J. Segschneider, and P. Wetzel (2005), The HAMburg Ocean Carbon Cycle Model HAMOCC5.1 - Technical Description Release 1.1, *Reports on Earth System Science*, *14*.

Marsland, S. J., H. Haak, J. H. Jungclaus, M. Latif, and F. Röske (2003), The Max-Planck-Institute global ocean/sea ice model with orthogonal curvilinear coordinates, *Ocean modelling*, *5*(2), 91–127.

Martin, J. H., G. A. Knauer, D. M. Karl, and W. W. Broenkow (1987), VERTEX: carbon cycling in the northeast Pacific, *Deep Sea Research Part A. Oceanographic Research Papers*, *34*(2), 267–285.

McCarthy, J. J., and E. J. Carpenter (1979), *Oscillatoria (Trichodesmium) Thiebautii (Cyanophyta)* in the Central North Atlantic Ocean, *Journal of Phycology*, *15*(1), 75–82.

Mohr, W., T. Grosskopf, D. W. Wallace, and J. LaRoche (2010), Methodological underestimation of oceanic nitrogen fixation rates, *PLOS one*, *5*(9), e12,583.

Moisander, P. H., R. A. Beinart, I. Hewson, A. E. White, K. S. Johnson, C. A. Carlson, J. P. Montoya, and J. P. Zehr (2010), Unicellular cyanobacterial distributions broaden the oceanic N_2 fixation domain, *Science*, *327*(5972), 1512–1514.

Monteiro, F., M. Follows, and S. Dutkiewicz (2010), Distribution of diverse nitrogen fixers in the global ocean, *Global Biogeochemical Cycles*, *24*(3).

Monteiro, F., S. Dutkiewicz, and M. Follows (2011), Biogeographical controls on the marine nitrogen fixers, *Global Biogeochemical Cycles*, *25*(2).

Moore, C. M., M. M. Mills, E. P. Achterberg, R. J. Geider, J. LaRoche, M. I. Lucas, E. L. McDonagh, X. Pan, A. J. Poulton, M. J. Rijkenberg, et al. (2009), Large-scale distribution of Atlantic nitrogen fixation controlled by iron availability, *Nature Geoscience*, *2*(12), 867–871.

Moore, J. K., and S. C. Doney (2007), Iron availability limits the ocean nitrogen inventory stabilizing feedbacks between marine denitrification and nitrogen fixation, *Global Biogeochemical Cycles*, *21*(2).

Moore, J. K., S. C. Doney, and K. Lindsay (2004), Upper ocean ecosystem dynamics and iron cycling in a global three-dimensional model, *Global Biogeochemical Cycles*, *18*(4).

Mulholland, M. R., and D. G. Capone (2000), The nitrogen physiology of the marine N_2-fixing cyanobacteria *Trichodesmium* spp., *Trends in plant science*, *5*(4), 148–153.

Najjar, R. G., X. Jin, F. Louanchi, O. Aumont, K. Caldeira, S. C. Doney, J.-C. Dutay, M. Follows, N. Gruber, F. Joos, et al. (2007), Impact of circulation on export production, dissolved organic matter, and dissolved oxygen in the ocean: Results from Phase II of the Ocean Carbon-cycle Model Intercomparison Project (OCMIP-2), *Global Biogeochemical Cycles*, *21*(3).

Needoba, J. A., R. A. Foster, C. Sakamoto, J. P. Zehr, and K. S. Johnson (2007), Nitrogen fixation by unicellular diazotrophic cyanobacteria in the temperate oligotrophic North Pacific Ocean, *Limnology and Oceanography*, *52*(4), 1317–1327.

O'Neil, J., and M. Roman (1994), Ingestion of the cyanobacterium *Trichodesmium* spp. by pelagic harpacticoid copepods Macrosetella, Miracia and Oculosetella, *Hydrobiologia*, *292*(1), 235–240.

Orcutt, K. M., F. Lipschultz, K. Gundersen, R. Arimoto, A. F. Michaels, A. H. Knap, and J. R. Gallon (2001), A seasonal study of the significance of N_2 fixation by *Trichodesmium* spp. at the Bermuda Atlantic Time-series Study (BATS) site, *Deep Sea Research Part II: Topical Studies in Oceanography*, *48*(8), 1583–1608.

Paerl, H. W., J. Huisman, et al. (2008), Blooms like it hot, *Science*, *320*(5872), 57.

Palmer, J., and I. Totterdell (2001), Production and export in a global ocean ecosystem model, *Deep Sea Research Part I: Oceanographic Research Papers*, *48*(5), 1169–1198.

Rodier, M., and R. Le Borgne (2008), Population dynamics and environmental conditions affecting *Trichodesmium* spp. (filamentous cyanobacteria) blooms in the south–west lagoon of New Caledonia, *Journal of Experimental Marine Biology and Ecology*, *358*(1), 20–32.

Rodier, M., and R. Le Borgne (2010), Population and trophic dynamics of *Trichodesmium* thiebautii in the SE lagoon of New Caledonia. Comparison with T. erythraeum in the SW lagoon, *Marine pollution bulletin*, *61*(7), 349–359.

Röske, F. (2005), Global oceanic heat and fresh water forcing datasets based on ERA-40 and ERA-15, *Tech. Rep. 13, Reports on Earth System Science*.

Sañudo-Wilhelmy, S. A., A. B. Kustka, C. J. Gobler, D. A. Hutchins, M. Yang, K. Lwiza, J. Burns, D. G. Capone, J. A. Raven, and E. J. Carpenter (2001), Phosphorus limitation of nitrogen fixation by *Trichodesmium* in the central Atlantic Ocean, *Nature*, *411*(6833), 66–69.

Sarangi, R., P. Chauhan, S. Nayak, and U. Shreedhar (2005), Cover: Remote sensing of *Trichodesmium* blooms in the coastal waters off Gujarat, India using IRS-P4 OCM, *International Journal of Remote Sensing*, *26*(9), 1777–1780.

Simmons, A., and J. Gibson (2000), The ERA-40 Project Plan, ERA-40 Project Report Series No. 1, ECMWF, *Reading, UK*, p. 63.

Six, K. D., and E. Maier-Reimer (1996), Effects of plankton dynamics on seasonal carbon fluxes in an ocean general circulation model, *Global Biogeochemical Cycles*, *10*(4), 559–583.

Smith, E. L. (1936), Photosynthesis in relation to light and carbon dioxide, *Proceedings of the National Academy of Sciences of the United States of America*, *22*(8), 504.

Sohm, J. A., and D. G. Capone (2006), Phosphorus dynamics of the tropical and subtropical North Atlantic: *Trichodesmium* spp. versus bulk plankton, *Marine Ecology-Progress Series*, *317*, 21.

Somes, C. J., and A. Oschlies (2015), On the influence of non-Redfield dissolved organic nutrient dynamics on the spatial distribution of N_2 fixation and the size of the marine fixed nitrogen inventory, *Global Biogeochemical Cycles*, *29*(7), 973–993.

Somes, C. J., A. Schmittner, and M. A. Altabet (2010), Nitrogen isotope simulations show the importance of atmospheric iron deposition for nitrogen fixation across the Pacific Ocean, *Geophysical Research Letters*, *37*(23).

Sonntag, S. (2013), Modeling biological-physical feedback mechanisms in marine systems, Ph.D. thesis, CRG Advancement of Coupled Climate Ocean Ecosystem Models, Research Area B: Climate Manifestations and Impacts, The CliSAP Cluster of Excellence, External Organizations.

Sonntag, S., and I. Hense (2011), Phytoplankton behavior affects ocean mixed layer dynamics through biological-physical feedback mechanisms, *Geophysical Research Letters*, *38*(15).

Takahashi, T., W. S. Broecker, and S. Langer (1985), Redfield ratio based on chemical data from isopycnal surfaces, *Journal of Geophysical Research: Oceans (1978–2012)*, *90*(C4), 6907–6924.

Taylor, K. (2001), Summarizing in a single diagram multiple aspects of model performance, *J. Geophys. Res*, *10*(6), 7183–7192.

Thomas, M. K., C. T. Kremer, C. A. Klausmeier, and E. Litchman (2012), A global pattern of thermal adaptation in marine phytoplankton, *Science*, *338*(6110), 1085–1088.

Vichi, M., N. Pinardi, and S. Masina (2007), A generalized model of pelagic biogeochemistry for the global ocean ecosystem. Part I: Theory, *Journal of Marine Systems*, *64*(1), 89–109.

Villareal, T., and E. Carpenter (2003), Buoyancy regulation and the potential for vertical migration in the oceanic cyanobacterium *Trichodesmium*, *Microbial Ecology*, *45*(1), 1–10.

Voss, M., H. W. Bange, J. W. Dippner, J. J. Middelburg, J. P. Montoya, and B. Ward (2013), The marine nitrogen cycle: recent discoveries, uncertainties and the potential relevance of climate change, *Philosophical Transactions of the Royal Society of London*

B: Biological Sciences, *368*(1621), 20130,121.

Walsby, A. (1978), The properties and buoyancy-providing role of gas vacuoles in *Trichodesmium* Ehrenberg, *British Phycological Journal*, *13*(2), 103–116.

Ward, B. A., S. Dutkiewicz, C. M. Moore, and M. J. Follows (2013), Iron, phosphorus, and nitrogen supply ratios define the biogeography of nitrogen fixation, *Limnol. Oceanogr*, *58*(6), 2059–2075.

Watanabe, S., T. Hajima, K. Sudo, T. Nagashima, T. Takcmura, H. Okajima, T. Nozawa, H. Kawase, M. Abe, T. Yokohata, et al. (2011), MIROC-ESM 2010: model description and basic results of CMIP5-20c3m experiments, *Geoscientific Model Development*, *4*(4), 845–872.

Weber, T., and C. Deutsch (2014), Local versus basin-scale limitation of marine nitrogen fixation, *Proceedings of the National Academy of Sciences*, *111*(24), 8741–8746.

Westberry, T., M. Behrenfeld, D. Siegel, and E. Boss (2008), Carbon-based primary productivity modeling with vertically resolved photoacclimation, *Global Biogeochemical Cycles*, *22*(2).

Westberry, T. K., and D. A. Siegel (2006), Spatial and temporal distribution of *Trichodesmium* blooms in the world's oceans, *Global Biogeochemical Cycles*, *20*(4).

White, A. E., Y. H. Spitz, D. M. Karl, and R. M. Letelier (2006), Flexible elemental stoichiometry in *Trichodesmium* spp. and its ecological implications, *Limnology and Oceanography*, *51*(4), 1777–1790.

Wolf-Gladrow, D. A., R. E. Zeebe, C. Klaas, A. Körtzinger, and A. G. Dickson (2007), Total alkalinity: The explicit conservative expression and its application to biogeochemical processes, *Marine Chemistry*, *106*(1), 287–300.

Zehr, J. P., J. B. Waterbury, P. J. Turner, J. P. Montoya, E. Omoregie, G. F. Steward, A. Hansen, and D. M. Karl (2001), Unicellular cyanobacteria fix N_2 in the subtropical North Pacific Ocean, *Nature*, *412*(6847), 635–638.

Zielinski, O., O. Llinás, A. Oschlies, and R. Reuter (2002), Underwater light field and its effect on a one-dimensional ecosystem model at station ESTOC, north of the Canary Islands, *Deep Sea Research Part II: Topical Studies in Oceanography*, *49*(17), 3529–3542.

Table 1. Model parameters related to the parameterization of prognostic N_2 fixers in experiment PROG.

Symbol	Variable	Value	Units
μ_{max}	Maximum growth rate	0.2	d^{-1}
m_{Diaz}	Decay rate	0.1	d^{-1}
$Diaz_{min}$	Minimum concentration	$1e^{-11}$	kmol P m^{-3}
w_{Diaz}	Buoyancy velocity	1.0	m d^{-1}
K_P	Half saturation constant for phosphate uptake	$1e^{-8}$	kmol P m^{-3}
K_{Fe}	Half saturation constant for iron uptake	0.32	nmol Fe m^{-3}
K_N	Half saturation constant for nitrate uptake	$1.6e^{-7}$	kmol N m^{-3}
$f_{DOM_{Diaz}}$	Fraction of DOM_{Diaz}	0.1	
f_{DET}	Fraction of detritus	0.9	
$rem_{DOM_{Diaz}}$	Remineralization rate of DOM_{Diaz}	$4e^{-5}$	d^{-1}
T_{opt}	Optimum temperature of growth	28.0	°C
T_1	Temperature window parameter 1	5.5	°C
T_2	Temperature window parameter 2	1.0	°C
α	Initial slope of P versus I curve	0.03	$d^{-1}(Wm^{-2})^{-1}$
k_r	Mean light attenuation coefficient of water for $\nu < 580$ nm	0.35	m^{-1}
k_w	Mean light attenuation coefficient of water for $\nu \geq 580$ nm	0.03	m^{-1}
k_{Chl}	Light attenuation coefficient of chlorophyll	0.04	m^2 (mg Chl)$^{-1}$
σ	Dividing PAR domain at 580 nm	0.4	
$R_{C:Chl}$	C:Chl ratio of N_2 fixers	60	g C (g Chl)$^{-1}$

Table 2. Globally integrated 100-year mean fluxes and inventories within the euphotic zone (except for N_2 fixation which is integrated over the whole depth range, and denitrification which includes the sediment) for the experiments REF and PROG.

Parameter	REF	PROG	Units
N_2 fixation	132.6	135.6	Tg N yr^{-1}
Denitrification (water column and sediment)	135.0	141.9	Tg N yr^{-1}
Primary production of bulk phytoplankton	61.01	45.53	Gt C yr^{-1}
Primary production of N_2 fixers		3.23	Gt C yr^{-1}
Export production at 90 m	7.24	7.46	Gt C yr^{-1}
Bulk phytoplankton biomass	0.62	0.61	Gt C
N_2 fixers biomass		0.10	Gt C
Zooplankton biomass	0.51	0.39	Gt C
Detritus biomass	1.62	1.57	Gt C
DOM inventory	5.88	4.64	Gt C
DOM_{Diaz} inventory		0.82	Gt C

Table 3. Applied values in the sensitivity experiments for the half saturation constants of phosphate K_P (left) and iron uptake K_{Fe} (middle), and the buoyancy velocity w_{Diaz} (right); and resulting values of N_2 fixation. The values with a gray background correspond to the reference run PROG.

Phosphate		Iron		Buoyancy	
K_P [kmol P m^{-3}]	N_2 fixation [Tg N yr^{-1}]	K_{Fe} [nmol Fe m^{-3}]	N_2 fixation [Tg N yr^{-1}]	w_{Diaz} [m d^{-1}]	N_2 fixation [Tg N yr^{-1}]
$0.1e^{-8}$	145.4	0.032	150.6	0	134.6
$0.5e^{-8}$	140.1	0.16	145.7	1	135.6
$1e^{-8}$	135.6	0.32	135.6	2	135.3
$2e^{-8}$	125.6	0.64	84.3	10	135.3
$10e^{-8}$	57.1	3.2	13.7	50	134.8

Figure 1. Top: Surface concentration of N_2-fixers biomass (mg C m^{-3}) **(a)** in the model (PROG, 100-year mean), and **(b)** in observations (0 - 10 m). Bottom: depth-integrated biomass (mg C m^{-2}) of N_2-fixers **(c)** in the model (PROG, 100-year mean) and **(d)** in observations. Observational data is taken from the database described in Luo et al. (2012), binned on a 3° x 3° grid. The geometric mean of each bin is shown.

Figure 2. Top: Surface N_2 fixation rates (μmol N m^{-3} d^{-1}) **(a)** in the model (PROG, 100-year mean), and **(b)** in observations (0 - 10 m). Bottom: depth-integrated N_2 fixation rates (μmol N m^{-2} d^{-1}) **(c)** in the model (PROG, 100-year mean) and **(d)** in observations. Observational data is taken from the database described in Luo et al. (2012), binned on a 3° x 3° grid. The geometric mean of each bin is shown.

Figure 3. (a) 100-year mean depth-integrated N_2 fixation (μmol N m^{-2} d^{-1}) in REF. (b) 100-year mean depth-integrated denitrification rate (μmol N m^{-2} d^{-1}) in PROG.

Figure 4. Growth limitation factors (100-year mean) of N_2-fixers in PROG: **(a)** iron (l_{Fe}), **(b)** phosphate (l_P), **(c)** temperature (l_T). **(d)** displays the total growth limitation (see Equation 3). Note that the limitation by light is not explicitly shown here.

Figure 5. **(a)** Vertical profiles of 100-year mean modeled N_2-fixers biomass (mg C m^{-3}) (green, upper x-axis), and N_2 fixation rates (μmol N m^{-3} d^{-1}) (red, lower x-axis), averaged over an area of 30°S to 30°N in PROG. **(b)** Vertical profiles of N_2 fixation rate at the station ALOHA, for PROG (red, 100-year mean), for REF (blue, 100-year mean), and for observations (black, mean and standard deviation of data from 2005 to 2010 taken from the database of Luo et al. (2012)).

Figure 6. Vertical section of 100-year mean zonally averaged N_2-fixers biomass (mg C m^{-3}) in PROG. The gray dashed line displays the zonally averaged mixed layer depth.

Figure 7. Seasonal evolution (100-year mean) of the vertical distribution of N_2-fixers biomass (mg C m^{-3}) in PROG on the northern hemisphere (NH) **(a)** and southern hemisphere (SH) **(b)**. The concentrations are averaged over an area of 40°N to the equator and 40°S to the equator, respectively. The gray dashed line displays the mixed layer depth averaged over the same area.

Figure 8. **(a)** Seasonal cycle of depth-integrated N_2 fixation (μmol N m^{-2} d^{-1}) at ALOHA: PROG (red, 100-year mean), REF (blue, 100-year mean), and observations (black, mean and standard deviation of data from 2005 to 2010 taken from the database of Luo et al. (2012)). **(b)** Surface N_2 fixation rates at BATS: PROG (red, 100-year mean), REF (blue, 100-year mean), observations (black, mean and standard deviation of approx. monthly data from 1995 to 1997 taken from the database of Luo et al. (2012)). Note the different scaling on the y-axis.

Figure 9. 100-year mean fields of nitrate (mmol N m^{-3}) at the surface (top), and at a depth of 100 m (bottom), in REF (left), PROG (middle), and observations (right).

Figure 10. 100-year mean fields of phosphate (mmol P m^{-3}) at the surface (top), and at a depth of 100 m (bottom), in REF (left), PROG (middle), and observations (right).

Figure 11. 100-year mean fields of P* (PO_4 - NO_3/16) at the surface (top), and at a depth of 100-250 m (bottom), in REF (left), PROG (middle), and observations (right).

Figure 12. Taylor diagram of nitrate (red), phosphate (green), oxygen (blue), and P* (black); at the surface (checkered) and at 100 m depth (filled); for the experiments PROG (crosses) and REF (circles). Global 100-year means of spatial correlations and standard deviations are shown. The observations (WOA 2013) are represented by a standard deviation and correlation of 1.

Figure 13. Depth-integrated N_2-fixers biomass (mg C m^{-2}) for the sensitivity experiments with varying half saturation constant for phosphate uptake (left, a-d), and iron uptake (right, e-h). Applied values from top to bottom: 0.1, 0.5, 2, and 10 times the original value of K_P=1e^{-8} kmol P m^{-3} and K_{Fe}=0.32 nmol Fe m^{-3} used in PROG.

Figure 14. Vertical section of zonal mean N_2-fixers biomass (mg C m^{-3}) with varying buoyancy velocities w_{Diaz}. From top to bottom: 0 m d^{-1}, 2 m d^{-1}, 10 m d^{-1}, 50 m d^{-1}.

Figure 15. Vertical profiles of mean N_2-fixers biomass (mg C m^{-3}) for varying buoyancy velocities w_{Diaz}, averaged over an area of 30°S to 30°N. Black: 0 m d^{-1}, red: 1 m d^{-1} (used in the reference run PROG), green: 2 m d^{-1}, blue: 10 m d^{-1}, light blue: 50 m d^{-1}.

Figure 1.

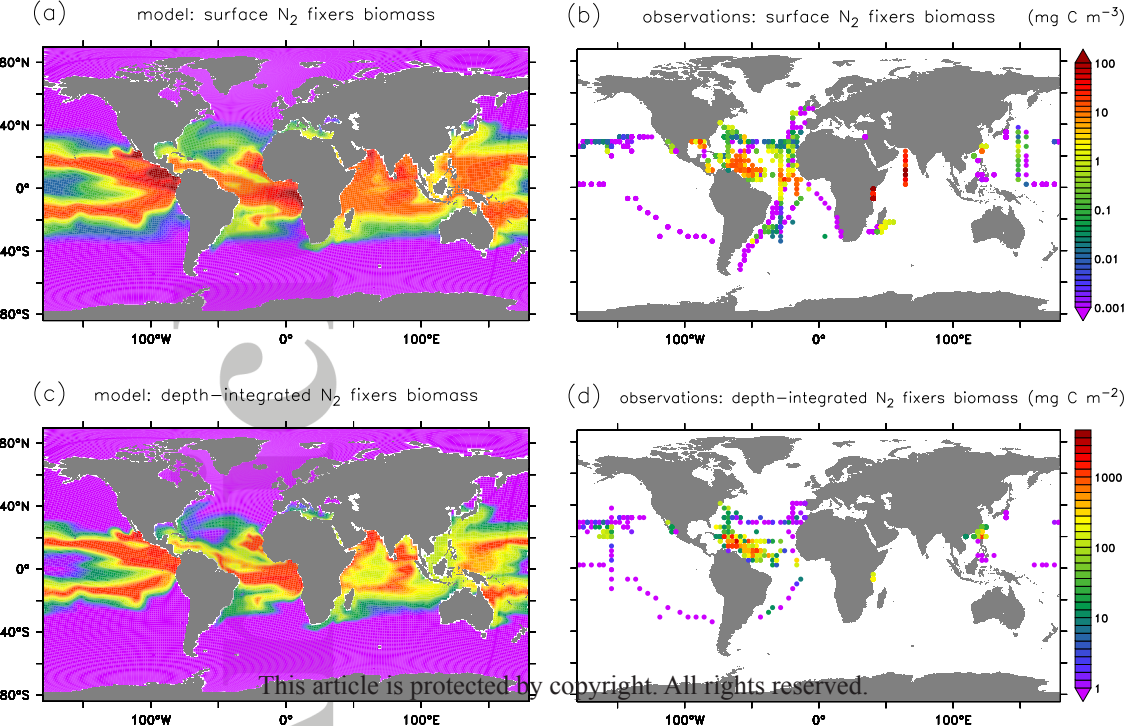

Figure 2.

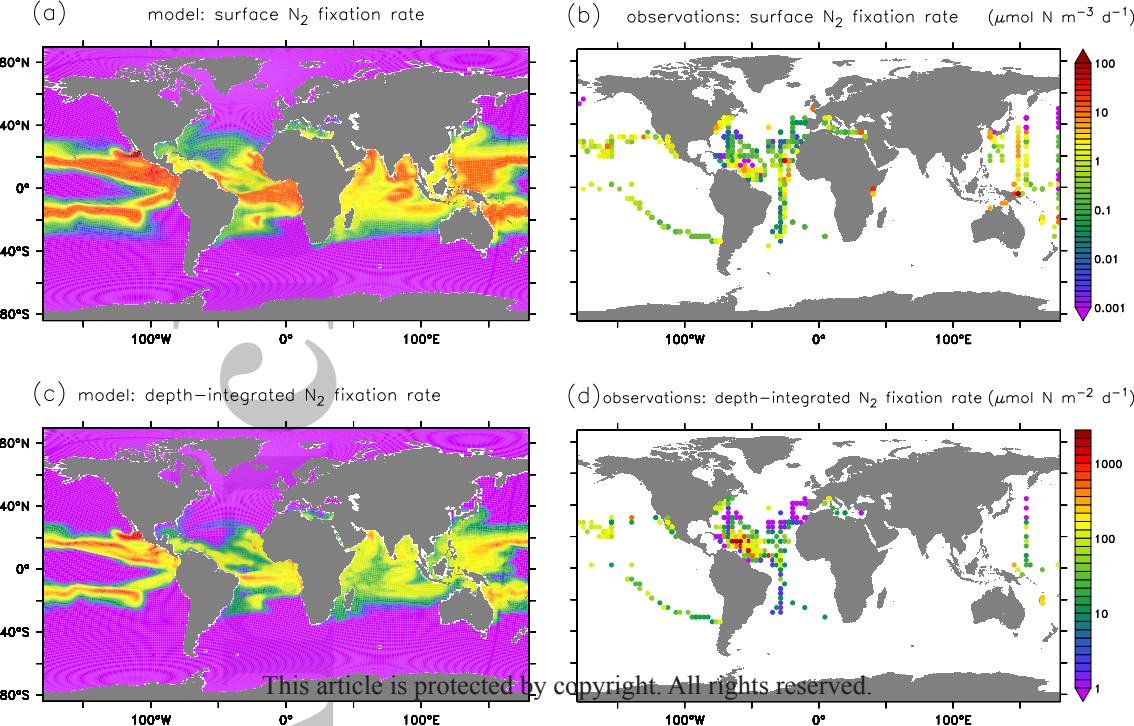

Figure 3.

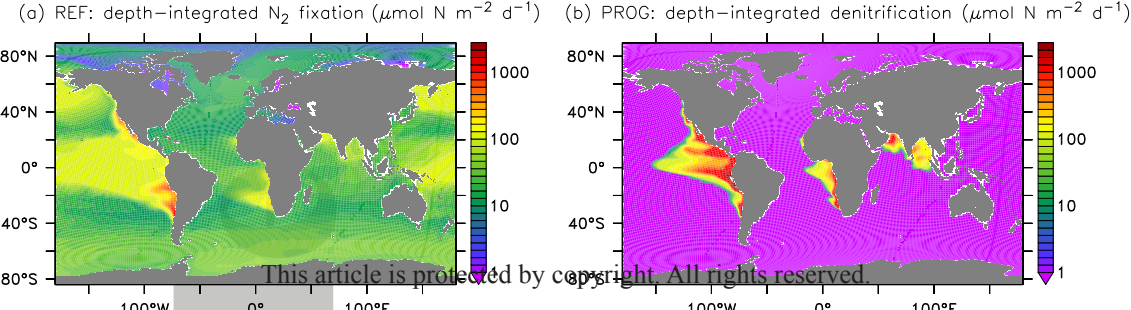

Figure 4.

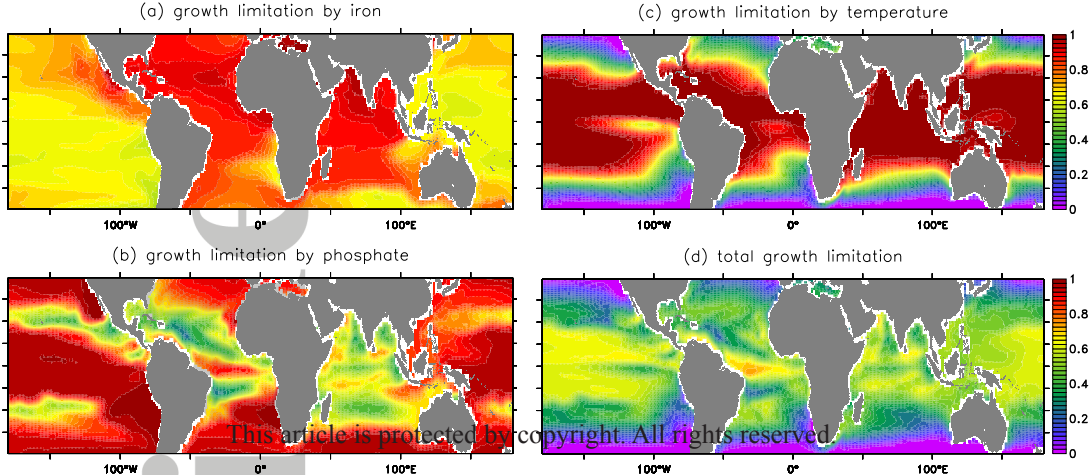

Figure 5.

(a) mean 30°S - 30°N

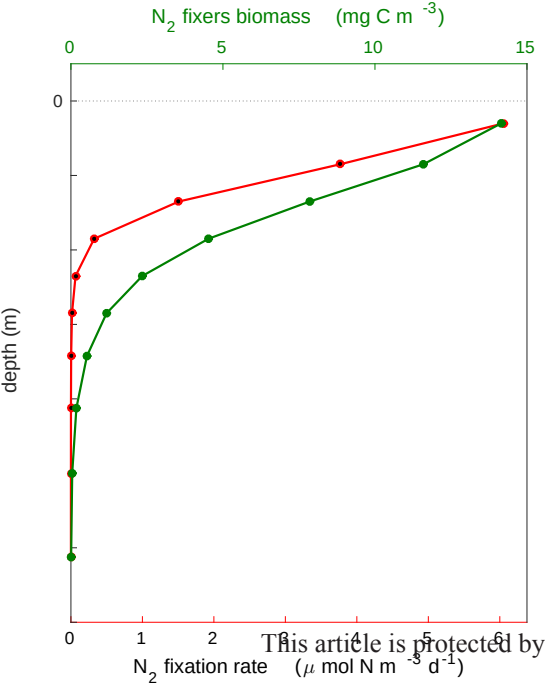

(b) ALOHA

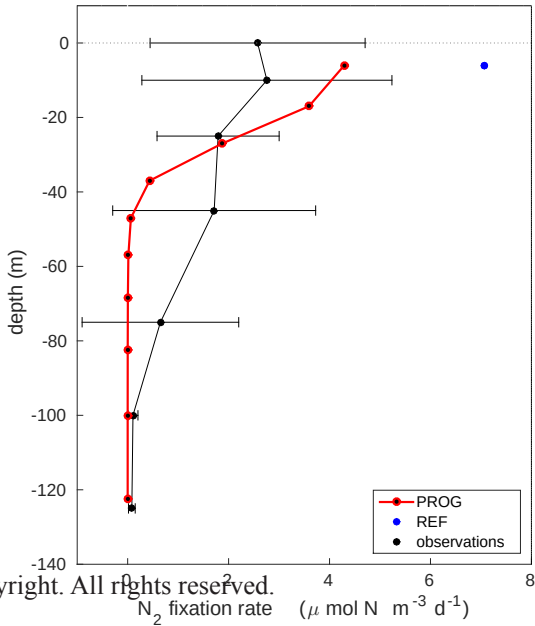

Figure 6.

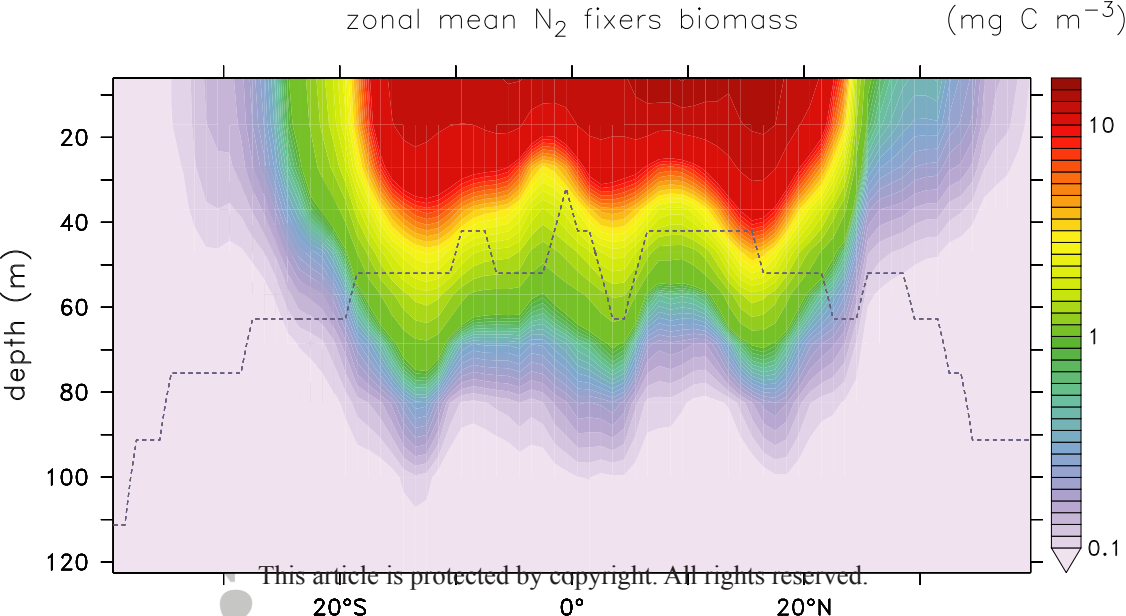

Figure 7.

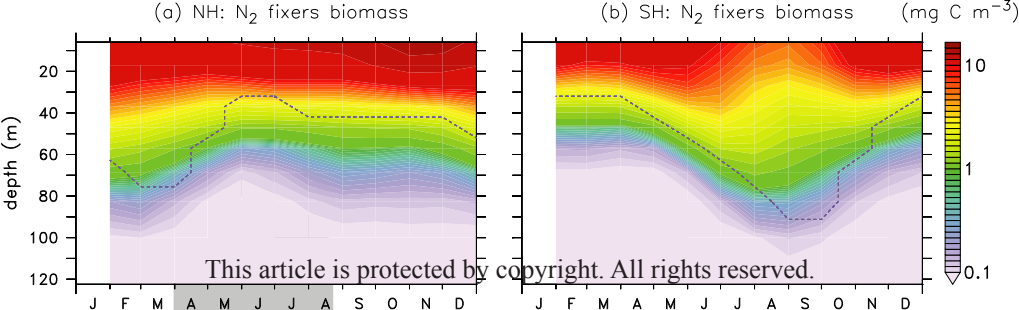

Figure 8.

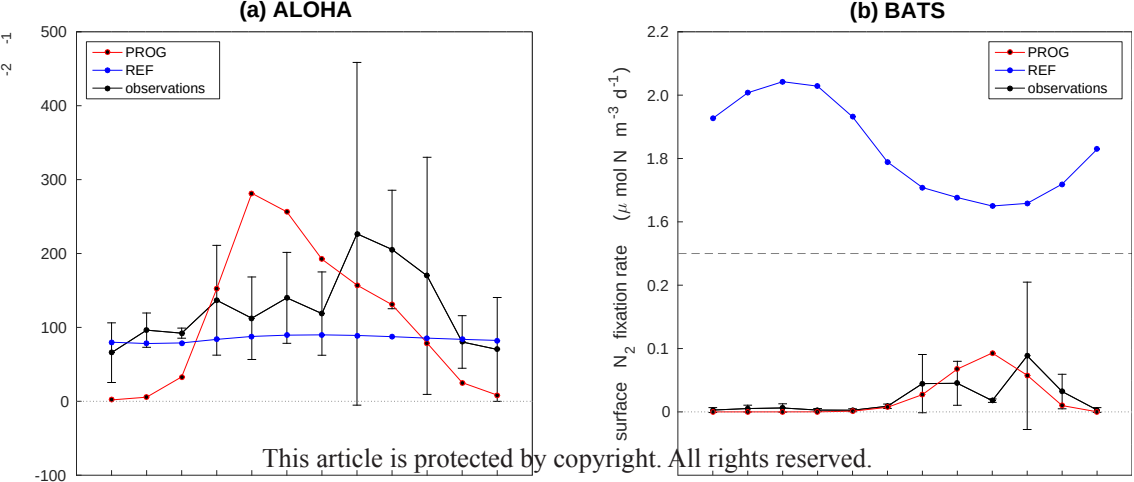

Figure 9.

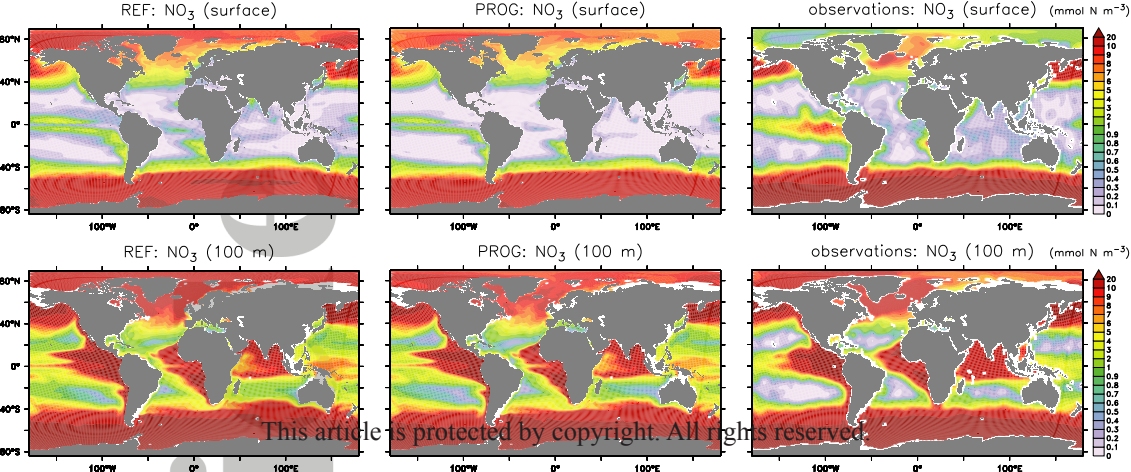

Figure 10.

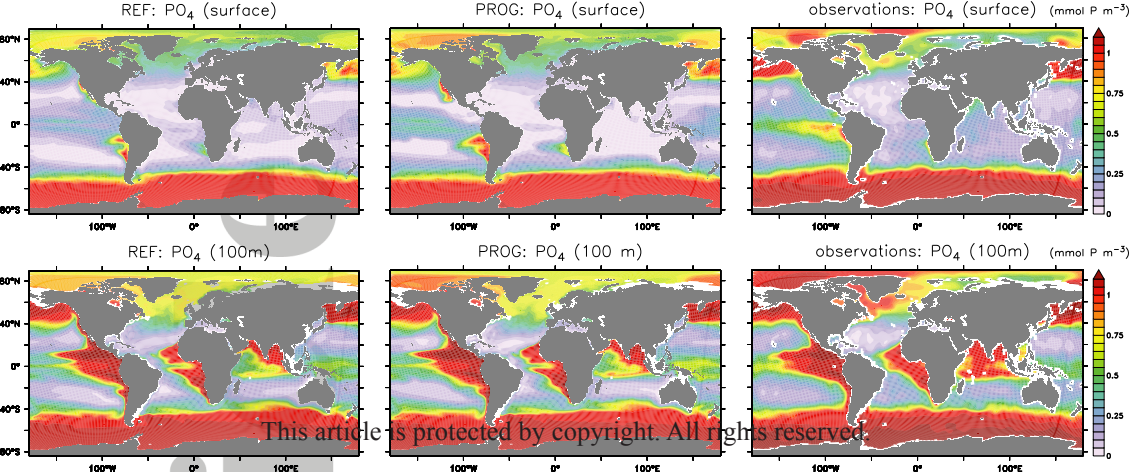

Figure 11.

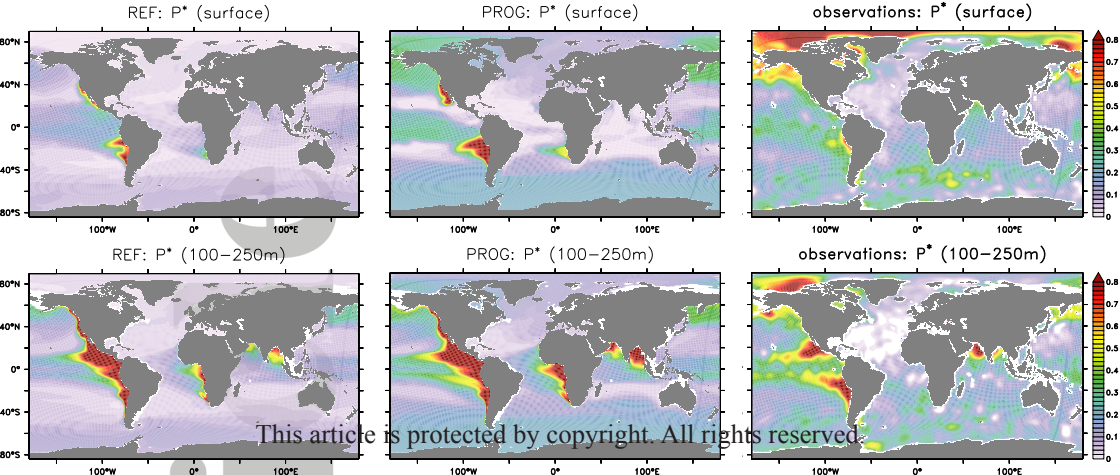

Figure 12.

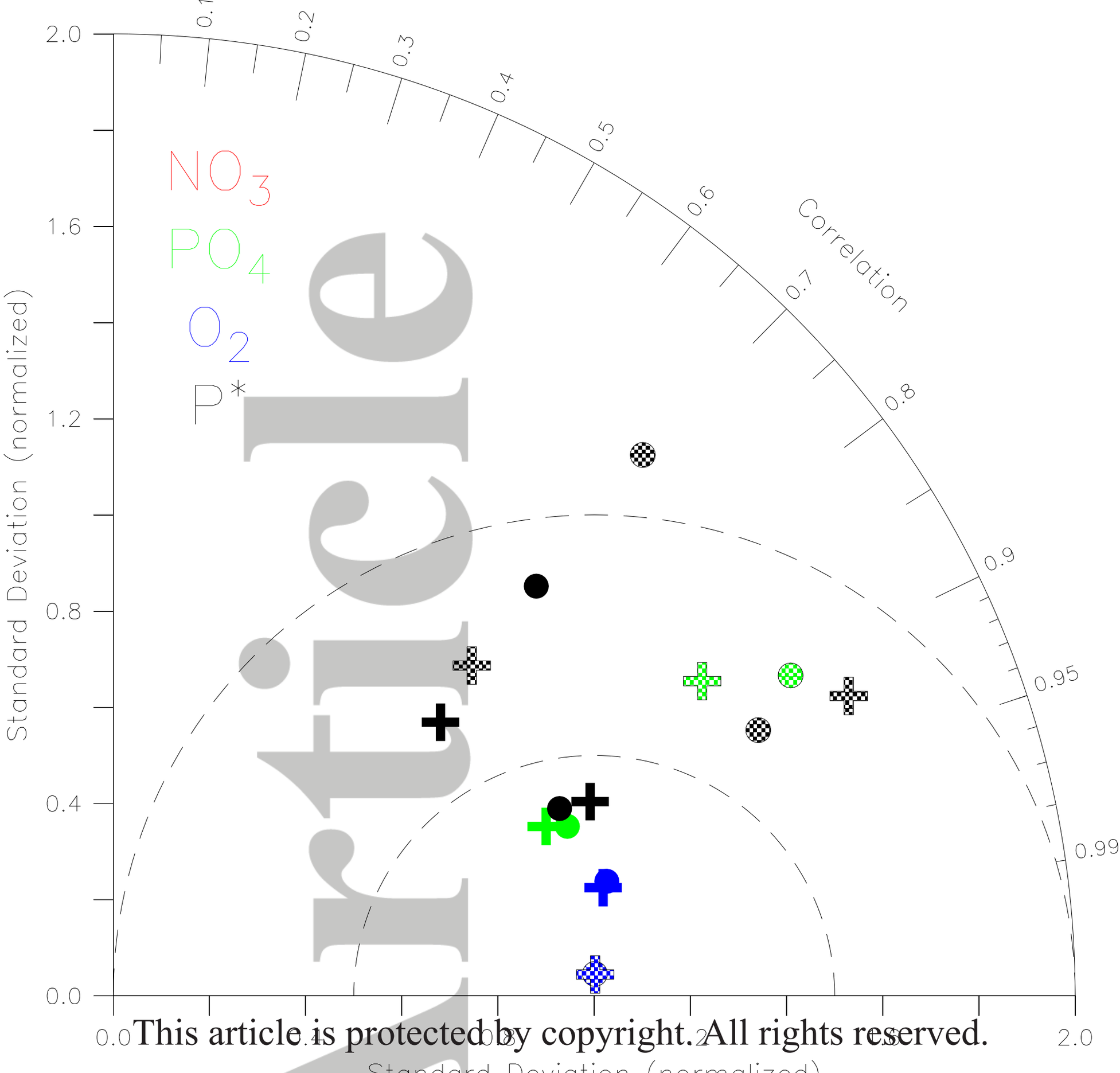

Figure 13.

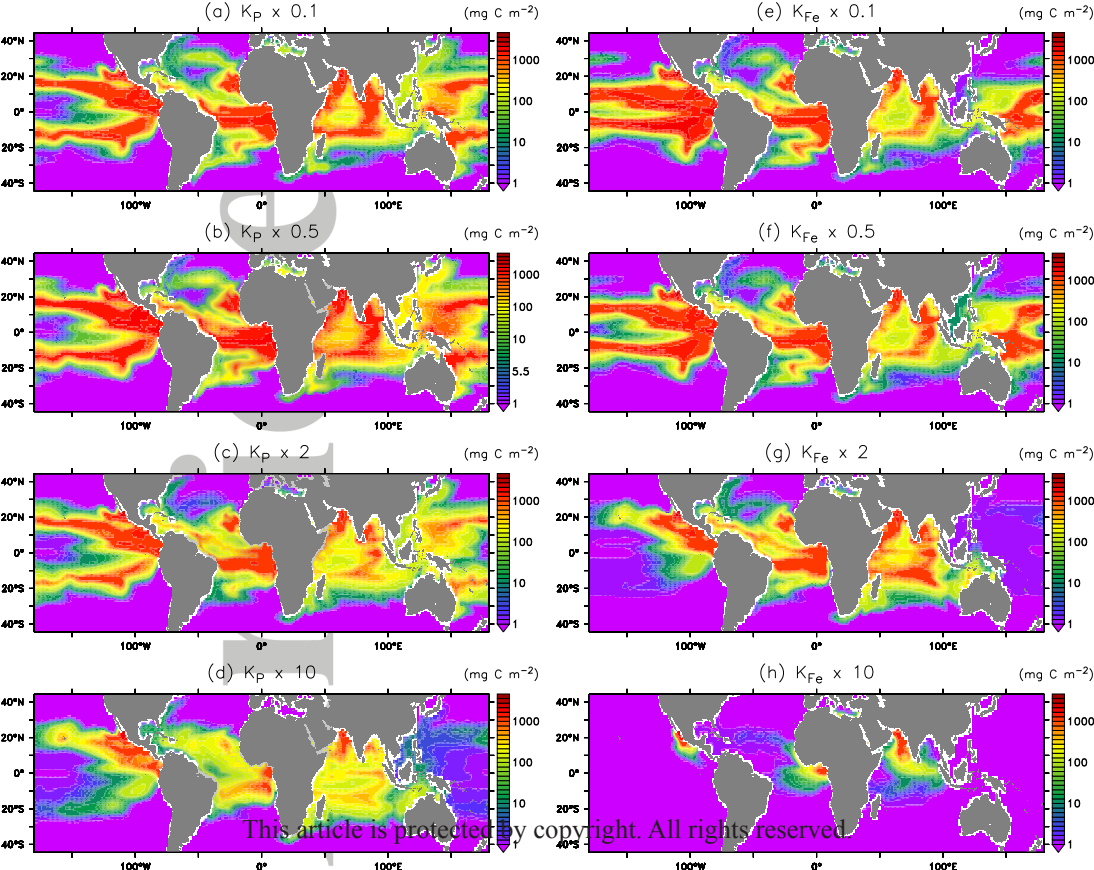

Figure 14.

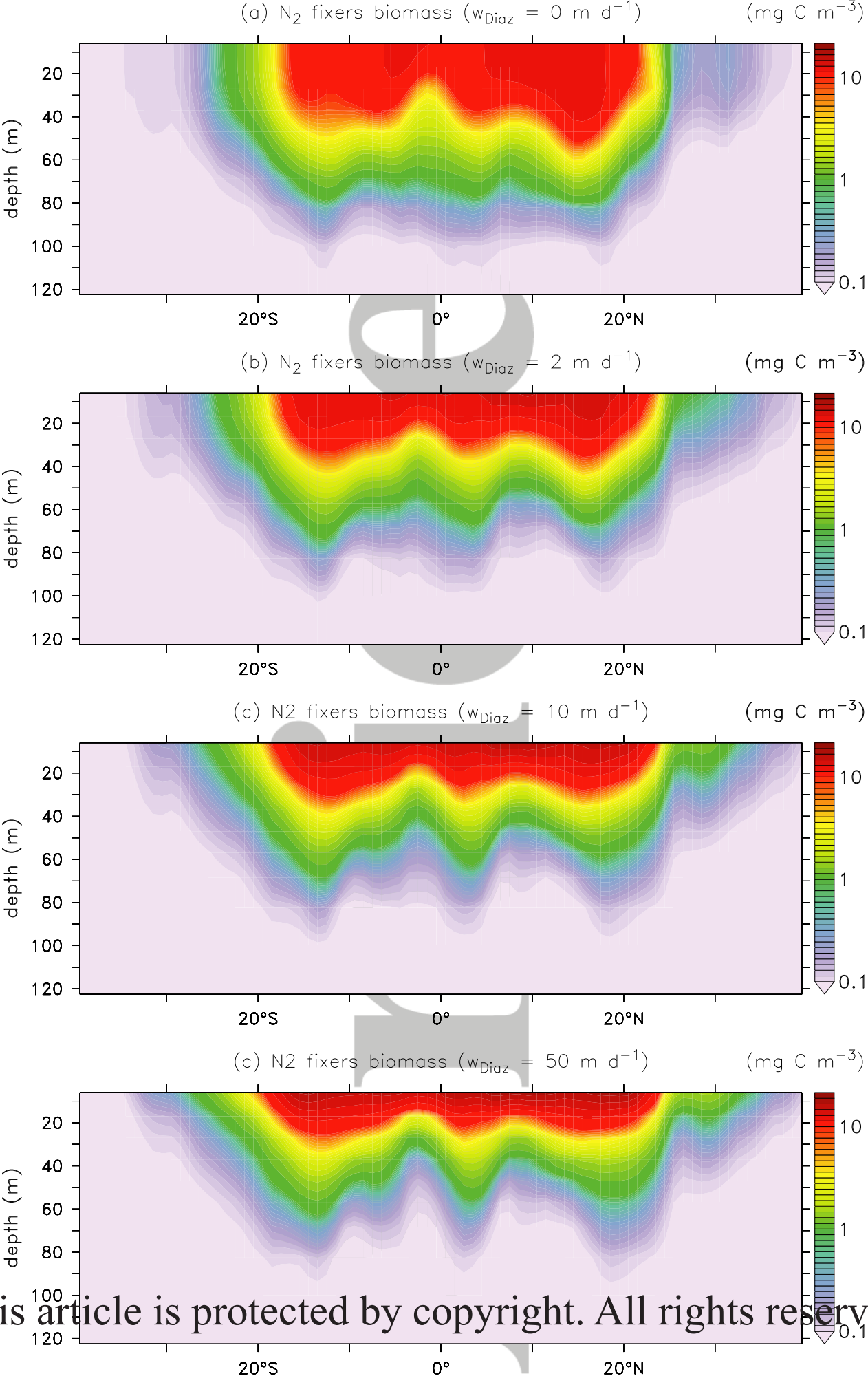

Figure 15.